Dark Cosmology Centre

Revealing the dynamics of Galaxy Clusters with X-rays

Master Thesis
at
Dark and Cosmology Centre
February, 4th of 2011

Catarina Silva Fernandes

Supervisor: Steen H. Hansen

Niels Bohr Institute

Faculty of Science, University of Copenhagen

Abstract

The study developed in this thesis concerns the dynamics of Galaxy Clusters. To estimate the total mass of a Galaxy Cluster we can rely on X-ray observations, and on the assumption of hydrostatic equilibrium. Galaxy clusters are known to be powerful cosmological tools, and measuring the total mass of different Galaxy Clusters is crucial to give us information on some of the cosmological parameters.

We propose a new method to constraint the Cluster's total mass from X-ray measurements, without relying on the assumption of hydrostatic equilibrium. This method relates the dynamics of the gas with the dynamics of dark matter particles in a Galaxy Cluster, and allow us to layout the dynamical state of the cluster. We apply this method to X-ray measurements of the Cluster A2052 and we find the difference between the total mass measured with this method, and the mass measured under the assumption of hydrostatic equilibrium, to be extremely significant. We also try to measure the gas velocity at the virial radius for this Cluster, and we constrain this to $|v_r| \leq (3.0 \pm 0.8) \times 10^2 km \cdot s^{-1}$.

Catarina Fernandes

catarina@dark-cosmology.dk

February, 4^{th} of 2011

Acknowledgments

First, I have to thank my supervisor Steen Hansen, for giving me the opportunity to work on this project, for all the ideas, motivation and guidance. For some of the technical details I would to thank Desiree Ferreira, Martina Zamboni and Teddy Frederiksen for being always available to discuss some of my questions. For the figures 1.2.1 and 4.1.1, I say "grazie" to Martina Zamboni and Martina Falco, respectively and "tak" to Steen Hansen for providing the reduced data for A2052.

To my mom for calling me almost everyday and my grandmother that misses me so much, for her strength. To my dear friends at home, for all the companionship, for making me feel always welcome and for the "saudade". To the Master students whom I shared the office with. For the spontaneous breaks, laughs, discussions, the long study nights and also for preventing my thesis to be lost in the e-world, a special thanks to Mitch for his comments. To sweet Lisbeth, whom in the last months made me feel as a daughter. I will cherish the moments spent organising old books at the NBI library and listening to the wonderful stories. To the dear Energy Crossroaders (Denmark), for their amazing presence. I can not thank enough to Allison, Ana, Karen and Ursula, for giving me shelter when in need of one.

I want to acknowledge the financial support of CIRIUS during the period when I was taking courses. I have to thank DARK for hosting me, for allowing me to borrow a laptop for the last two months, for the coffee and cookies. Thanks to all at DARK, for the welcome environment, it has been a pleasure to be here and learn so much about Astrophysics.

Last, but by no means less important, I acknowledge the loss of the trees that gave me so much knowledge, and the others that only got to be draft paper.

Contents

Chapter 1

Introduction

Our thirst for knowledge is never ending. Most of us are fascinated by what is out there, when, how did everything start, how is the universe organised. We now know that surrounding this planet, there are other planets and stars. Not even our galaxy is alone and at night, if the sky is clear, one can catch a glimpse of Andromeda galaxy with the naked eye or if you happen to be in the southern hemisphere, to the Large Magellanic Cloud - an irregular galaxy, that along with our galaxy, Andromeda and other galaxies form the Local Group. As the Local Group, there are also other collections of galaxies, also known as clusters of galaxies. These clusters are known to be the largest gravitationally bound objects in the universe and are the subject of study for this thesis.

In this Introduction we set the scene for this thesis work. References for the introduction are Binney [4], Dodelson [12] and Freeman [19].

1.1 Scaling towards galaxy clusters

It all started at a singularity, with the Big Bang. As the universe expanded it also cooled down and when the temperature of the gas was of a few hundred kelvin, the first electrically neutral atoms started to form. The photons, that before were scattered by collisions with charged particles, could then start to travel freely through space. These photons have come a long way and we can now measure them from the Cosmic Microwave Background (CMB). After approximately 10^9 years, the primordial atoms started to clump together and the first stars were formed. In the hierarchical merging scenario, large scale structures formed by merging of smaller objects, due to gravitational attraction. Stars and gas agglomerated into galaxies. Gravitationally bound galaxies then agglomerate into what we call a cluster of galaxies. Such clusters are formed by the infall of clumps along filaments and are still forming at the present epoch [31].

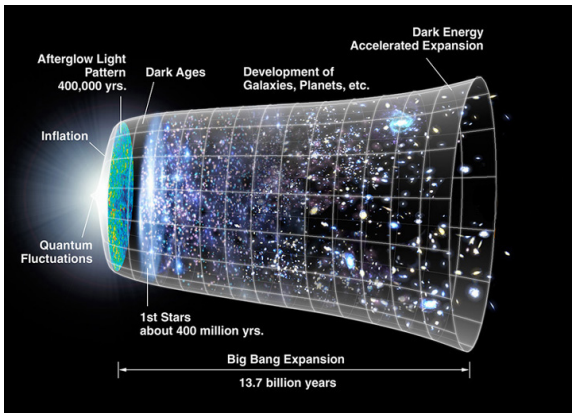

Figure 1.1.1: Representation of the evolution of the universe at different epochs since the Big Bang. General Relativity starts to be valid after quantum fluctuations, early before the CMB was emitted. Current cosmological models such as the FRW universe ($a(t) \propto t^q$, a is the cosmic scale factor), predict that it all started with an initial singularity, the Big Bang (singularity when $t \to 0$ $a \to 0$). At early times radiation dominated ($q = 1/2$), at later times non-relativistic matter dominates ($q = 2/3$) and we now have a universe which is dominated by dark energy, Λ. This energy can be interpreted as the vacuum-energy. Image from NASA webpage.

1.1.1 Probing the universe

Galaxy clusters are the largest gravitationally bound objects in the universe. Typically, matter inside these clusters is comprised of 75% dark matter, 20% of hot diffuse intra cluster plasma and 5% of stars, dust and cold gas being mostly tied to galaxies. Overall their mass[1] is of the order of $\sim 10^{13} - 10^{15}$ $M_\odot$ and size[2] of $\sim 10^3$ kpc.

Galaxy clusters are spectacular [21] and are powerful cosmological tools as they mark the transition between large and smaller scales [7]. In particular, they can set constraints on the matter density parameter Ω_m, [3] see fig. 1.1.2.

Preferably, one should study how clusters evolve in cosmological time scales, but these are just too long. For this reason, it becomes relevant to look at how an entire population of clusters, with the same mass, changes with redshift, z. The mass function $n(M, z)$ gives the number density of virialised halos (where the virial theorem holds) found at redshift z with mass in the range $[M, M + dM]$.

Thus, if we want to set better constraints on this parameter, it is crucial that the cluster's total mass is estimated at different redshifts with the highest accuracy possible [41].

[1] $1\ M_\odot = 1.98 \times 10^{30}$ kg.

[2] 1 kpc $= 1 \times 10^{19}$ m.

[3] For details on how to obtain Ω_m and relating it to the mass function from σ_8, refer to the Press-Schechter formalism, chapter 9.5 in Dodelson [12].

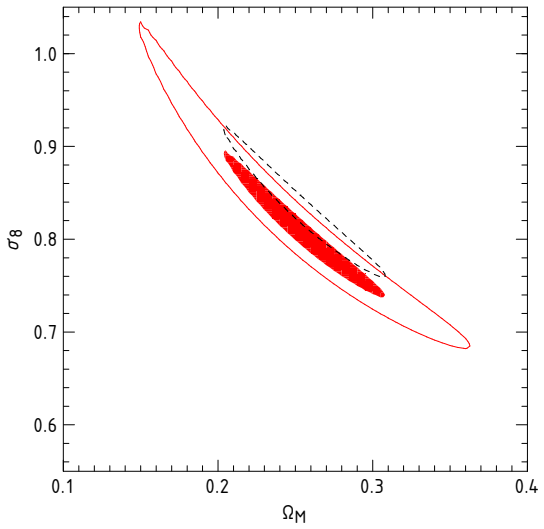

Figure 1.1.2: Constraints on σ_8 and Ω_m parameters in a flat ΛCDM cosmology from a cluster sample (both low and high-redshift), and σ_8 is the amplitude of linear perturbations at the length scale $8h^{-1}$ Mpc and is given from cluster abundances. Image by Vikhlinin [3].

Dark Matter

To prevent the cluster from gravitational collapse, it is necessary that the kinetic energy from particle's motion balances the gravitational one. The system will then settle into an equilibrium condition. This is the same as saying that the object is virialised or that the Virial theorem holds: $2\langle E_{kin}\rangle + \langle E_{pot}\rangle = 0$. We can then apply this theorem to galaxies, and by measuring the motion of the particles inside a galaxy it becomes possible to infer the total mass of the system: $M_{Total} = r_G \langle v^2\rangle / G$, with r_G being the gravitational radius[4] and $\langle v^2\rangle$ the evaluated velocity dispersion[5].

In the last century this theorem allowed astronomers to postulate the existence of dark matter as the total gravitational mass obtained from dispersion velocity measurements was different (higher) than the one expected purely from the luminosity mass. The presence of dark matter halos can also explain the rotation curve of luminous matter in a galaxy.

The composition of this missing matter is currently unknown, but some of the best candidates are neutrinos or WIMPS (weakly interactive massive particles). So far, the detectors that are searching for a dark matter particle have shown no signal of it. Dark matter halos can be modelled by the following double-power law:

$$\rho(r) = \frac{\rho_0}{\left(\frac{r}{a}\right)^{\alpha}\left(1+\frac{r}{a}\right)^{\beta-\alpha}} \tag{1.1.1}$$

[4] $r_G \sim 1$ Mpc. 1 Mpc $= 3.08 \times 10^{22} m$. Gravitational constant, $G = 6.673 \times 10^{-11} m^3 kg^{-1} s^{-2}$.
[5] $\langle v^2\rangle = 3\sigma_r^2$, where σ_r^2 is the radial velocity dispersion.

with $(\alpha, \beta) = (1, 3)$ gives the Navarro-Frenk-White (NFW) profile, predicted by N-body simulations [29], with two free parameters ρ_0 which is the central dark matter density and a the scale radius.

1.2 The problem at hand

With this thesis, we want to describe a method that can possibly give us more knowledge about how dark matter is distributed. At the same time, we also want to try and see if it is possible to get some insight about the cluster dynamics. Such a comparison between the dark matter distribution and the cluster's complete dynamics has not been done before taking X-ray observations only, which makes this project so exciting.

A critical point will be to estimate the total mass of the cluster. For that we could rely on different methods apart from X-rays such as studying the motion of galaxies or using weak-gravitational lensing (WGL).

Galaxy motion

Even though it is possible to make an estimation of the mass of a galaxy by measuring the galaxy's velocity dispersion, the same is not so easy for real clusters as they are not isolated systems, thus we can not consider clusters to be in a steady state. For example, we can have infalling of matter into the cluster at the cluster's outskirts.

General idea of WGL

Galaxy clusters are massive bodies, and as such, according to Einstein's theory of General Relativity, the cluster's gravitational field will curve space-time. The principle behind lensing is that since light (and matter) always take the shortest path (geodesic), if the geodesic is curved due to the presence of the cluster, their path along it will curve for the observer. When we have a background radiation from a source object behind the cluster, we will have a distorted image from light passing in the cluster's neighbourhood. The amount of distortion will tell us about the cluster's total gravitational mass which is biased by any mass distributed along the line-of-sight as it will also affect the photon's path.

Zhang et al.[43] tried to compare this method with the one applied for X-ray observations (under the assumption of hydrostatic equilibrium) to see how different the mass estimations are, and they found that they can diverge by $\sim 10 - 40\%$. However, the uncertainties on weak-lensing mass estimates can be 10-50% which does not make it a good method for what we are trying to achieve.

X-ray measurements

With temperatures of the order of 10^7 K, the gas in the intra-cluster medium (ICM) of the cluster is fully ionised, giving it the properties of plasma. At that temperature the cluster emits X-rays ($k_BT \sim$ keV) due to Bremsstrahlung effect (see app.B.1). Due to this effect, the emissivity depends on the electron density (n_e) and on the temperature (T) in such fashion: $\epsilon_\nu \propto n_e^2 T^{1/2} \exp(-E/T)$.

Fig. 1.2.1 shows us a X-ray spectrum obtained from counting photons and its energy at a certain distance from the centre of the cluster. From the spectra we see that its shape follows an exponential: $I_\nu \propto \exp(-h\nu/k_BT)$. [6]

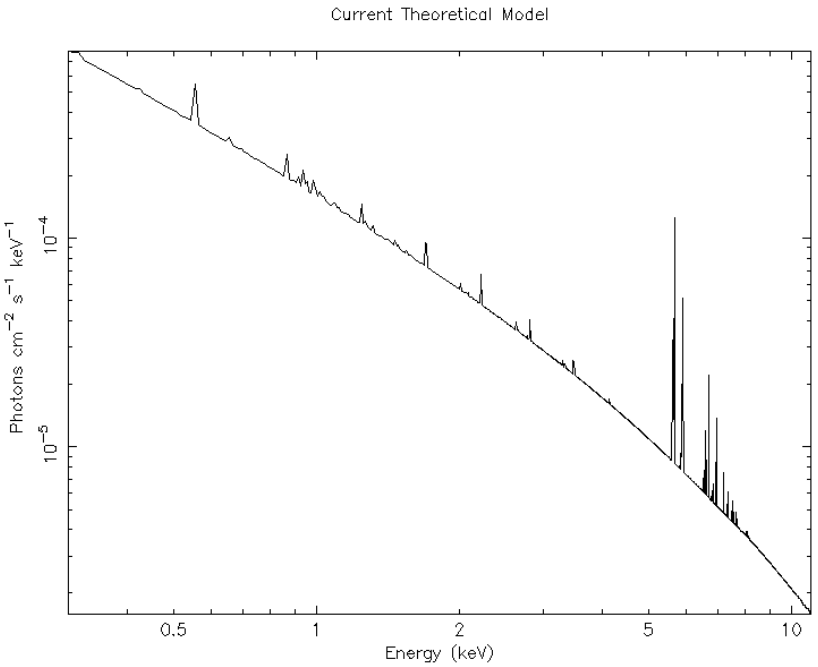

Figure 1.2.1: X-ray energy spectrum obtained from XSPEC in log-log scale. The x-axis corresponds to the energy of the photons in keV and the y-axis to the normalised surface brightness. The lines are related to the metallicity of the cluster, and with it we are able to calculate the redshift for the cluster (see app. B.1). From the continuum, we estimate the number density from the normalisation and temperature for the gas from the shape of the spectrum.

From observations we would like to have access to regions close to the virial radius, which is taken to be approximately R_{200}. R_Δ is defined to be the radius at which the enclosed spherical over density is $\rho(r) = \Delta \times \rho_c$, ρ_c is the critical density of the universe at the cluster's redshift: $\rho_c = \frac{3H(t)^2}{8\pi G}$, [7]. Typical values for R_Δ are $R_{2500}(\sim 0.25\ R_{200}) \sim 500$kpc, $R_{500} \sim 10^3$kpc and $R_{200} \sim 2 \times 10^3$kpc. With today's

[6] h - Planck's constant. k_B - Boltzmann's constant.

[7] H - Hubble constant at the cluster's redshift.

X-ray telescopes we trust data from cluster centric distance R_{2500} as far as to R_{500}, in a near future it will be possible to get information about the cluster up to R_{200}, where the cluster is still forming.

Density profile

The surface brightness can be modelled to the β and Sérsic model for non-cool core clusters (NCC) and cool core clusters (CC), respectively [26]. Here we write the correspondent density profiles which can be obtained by deprojecting its surface brightness[8]. First the β-profile:

$$\rho_g(r) = \rho_0 \left(1 + \frac{r^2}{r_c^2}\right)^{-3\beta/2} \tag{1.2.1}$$

where ρ_0 and r_c are the central gas density and core gas radius, respectively and β is the shape parameter [11].

If we were to consider a β-model for a CC cluster, what would happen is that the mass derived from hydrostatic equilibrium (2.2.9) would turn out to be negative close to the central region as the temperature decreases towards the centre. Which is of course a non-physical solution. One may instead use the Sérsic-model to model the gas density for such clusters:

$$\rho_g(r) = \rho_0 \left(\frac{r}{r_s}\right)^{-p\prime} \exp\left[-\left(\frac{r}{r_s}\right)^{\nu}\right] \tag{1.2.2}$$

where $p\prime$ is correlated with ν, a shape parameter: $p' = p/2$, $p = 1 - 0.6097\nu + 0.05563\nu^2$, $r_s = r'_s 2^{1/\nu}$ and r'_s being the scale parameter [15].

Temperature profile

To determine the temperature, there must be enough source counts to ensure a good signal-to-noise ratio. The temperature can be obtained from the fitting of the spectrum (fig. 1.2.1). Again, with deprojection techniques we will have a measurement of the temperature for each radial bin.

Total Mass

Having access to the gas density and temperature and how its gradient varies along the cluster, it is possible to estimate the cluster's total mass assuming the gas in the ICM to be spherical and in hydrostatic equilibrium. Such estimation on the cluster's total mass have 10% accuracy with current telescopes from *Chandra* and *XMM-Newton* [17].

[8]Deprojection is like making onion peeling, and we will have to do spectra subtraction to get information at different radii.

For real clusters it is unlikely to have such perfect equilibrium state. Moreover, outside the scope of X-ray observations are the detection of magnetic fields and cosmic rays which also contribute to the cluster's dynamics.

1.2.1 Magnetic fields and Cosmic Rays in Galaxy Clusters

There is observational evidence that magnetic fields and cosmic rays are present in all clusters. As cluster mergers are the most energetic events in the universe, it is believed that they power the mechanisms responsible for the origin of these non-thermal components in clusters. A fraction of the energy dissipated during these mergers is expected to be channelled into the amplifications of magnetic fields and into the acceleration of particles via shocks and turbulence [9].

Magnetic Field

It is still not clear how magnetic fields arise in cluster of galaxies, or how their structure and magnitude behave[25].

Magnetic fields are created by moving electric charges [9]. The origin of these magnetic fields is nowadays one of the most challenging problems in astrophysics, and observations are still poor. Different measurement methods are described in app.(B.3). Some of the discussion about origin of seed fields in clusters refers to the Biermann battery effect in shocks [42], galactic outflows and jets[10].

The Biermann battery effect goes way back to mergers and shocks related to the hierarchical structure formation which give rise to small electric currents and may generate magnetic fields. Due to the large conductivity of the ICM these are extremely weak magnetic fields ($\sim 10^{-20}$ G, [11]). Other arguments such as the high metallicity observed in the ICM suggests a significant enrichment that must have occurred in the past (low redshift ($z \sim 2-3$)) due to galactic winds or active galactic nuclei (AGN) giving rise to magnetic fields $\sim 0.1 \times 10^{-6}$ G. The winds and jets produced can then carry the magnetic fields through the ICM.

Current measurements of magnetic fields in galaxy clusters are of the order of 10^{-6} G, suggesting amplification of these seed fields.

Cosmic rays

Cosmic rays is the name given to relativistic particles. Non-thermal electrons such as cosmic ray (CR) electrons can be observed directly via their radio synchrotron emission (see appendix (B.2)), forming the cluster radio halos. In the same way as moving charged particles create a magnetic field, the presence of such a field will induce charged particles (e.g., CR electrons) to move.

[9] Electric fields that vary in time, recall Maxwell's equations.
[10] Further reading in Dolag et al.[13].
[11] G - unit of gauss. In SI: 1 G = 10^{-4} T.

From the radio signature, via synchrotron emission, it is known that the CR electrons and protons can be injected into the ICM mainly by three different processes: acceleration by shock waves from structure formation; re-acceleration from winds; gas stripping due to sources in the host galaxy such as radio galaxies, supernovae or AGN [32].

The associated cooling time of the CR electrons $\sim 10^2 yr$ tell us that these CR electrons must have been recently injected or re-accelerated. On the other hand, CR protons have long radiative lifetimes in the ICM of the order of Hubble time which allows them to be as old as the cluster itself. A CR protron can collide inelastically with a nucleon (N) of the ICM (approximately once in a Hubble time that can happen) where secondary particles such as secondary CR electrons and γ rays are produced according to the following reaction chain [16], [12]:

$$p + N \rightarrow 2N + \pi^{\pm/0} \tag{1.2.3}$$

$$\pi^{\pm} \rightarrow e^{\pm} + \nu_e/\bar{\nu_e} \tag{1.2.4}$$

$$\pi^0 \rightarrow 2\gamma \tag{1.2.5}$$

Secondary CR electrons can be observed from the same radiation processes as the primary ones. Gamma rays (γ) can be detected in the future with better gamma-ray telescopes.

1.2.2 Summary

In summary, we want to measure the cluster's total mass accurately from X-ray observations alone since this is the best method so far. Observations are not able to tell us about the gravitational mass of the cluster, since we can not observe dark matter. For this reason, we will have to study its dynamics.

Usually, one considers the gas in the ICM to be spherical and in hydrostatic equilibrium. This assumption may not be always true because the cluster's dynamics can be influenced from the presence of magnetic fields, cosmic rays and the gas velocity[13]. Therefore, the mass given from direct X-ray measurements under this usual assumption may not be the true dynamical mass of the cluster.

Our goal is to derive a method that takes the data from X-rays observations and estimates the mass of the cluster. This method shall be different assuming hydrostatic equilibrium. We propose such method by also studying the dark matter halo.

We will then take the difference between the cluster's true mass and compare it with the hydrostatic mass. The difference between the two masses should tell us something about the magnetic field, cosmic rays or the gas' velocity distribution along the cluster.

[12] We are not writing the decay of the pion into a muon and a muon neutrino.

[13] In the case of not static: $\frac{d\mathbf{v}}{dr} \neq 0$

Chapter 2

Galactic Cluster Dynamics

In this chapter we show how to obtain an estimation on the total mass for the cluster and its dynamics. I will start with the collisionless dynamics for dark matter particles present in the cluster. This will lead us to Jeans' equation.

Another way to estimate the total mass of the cluster will be to study the gas in the ICM. As it is fully ionised, we can consider it to be a fluid. With this description we will for now assume that the gas is static and only thermal pressure (from the gas) is acting against gravitation.

If the reader prefers to skip the technical details of these two derivations, then go to page 18 where the Jeans' and the hydrostatic equilibrium equation are again explicitly written.

2.1 Collisionless dynamics

Numerical simulations show that dark matter should be mostly cold and collisionless. We combine the notes from Binney [4] and from lectures in Advanced Cosmology[1] to describe such dynamics and how the cluster's total mass can be derived.

2.1.1 DF and CBE

In 3D we can define some point in space to have a certain amount of solar masses per cubic parsec which would be difficult to measure. Therefore, to describe an ensemble of collisionless particles we go to phase-space where we should then consider the phase-space coordinates $\mathbf{w} = (\mathbf{x}, \mathbf{v})$ in 6D [2]. The probability of finding a dark matter particle inside an infinitesimal volume $d^3\mathbf{x}d^3\mathbf{v}$ is given by the distribution function (DF) $f(\mathbf{w}, t)d^6\mathbf{w}$ and evolves with time as particles move in phase-space. These dark matter particles do not suffer from collisions, therefore they can not jump from one point to another but move smoothly throughout phase-space. From statistical

[1] Lectured by Steen Hansen, 2010.

[2] We use the notation in bold when referring to a vector.

mechanics we know that the evolution of the DF for a collection of particles is given by the Boltzman equation which in the case of no collisions is:

$$\frac{df}{dt} = \frac{\partial f}{\partial t} + \frac{\partial (f\dot{w_\alpha})}{\partial w_\alpha} = 0 \tag{2.1.1}$$

This equation is formally known as collisionless Boltzmann equation (CBE) and is the starting point to derive the Jeans equation. Here we are using Einstein's notation where $\alpha = 1, 2, ..., 6$ and $i = 1, 2, 3$ unless otherwise stated. The third term can be expanded, which will lead us to:

$$\frac{\partial (f\dot{w_\alpha})}{\partial w_\alpha} = \dot{w_\alpha}\frac{\partial f}{w_\alpha} + f\left(\frac{\partial v_i}{\partial x_i} + \frac{\partial \dot{v_i}}{\partial v_i}\right) \tag{2.1.2}$$

The velocity does not explicitly depend on the position and from the equation of motion, $\dot{v_i} = -\frac{\partial}{\partial x_i}\Phi$, with Φ being the gravitational potential. Assuming that the potential only depends on position and time, we can see that the term inside the curved brackets will be equal to zero, and the CBE (2.1.1) becomes:

$$\frac{\partial f}{\partial t} + \left(\dot{x_i}\frac{\partial f}{\partial x_i} + \dot{v_i}\frac{\partial f}{\partial v_i}\right) = 0 \Rightarrow \frac{\partial f}{\partial t} + \mathbf{v}\cdot\boldsymbol{\nabla} f - \boldsymbol{\nabla}\Phi\cdot\frac{\partial f}{\partial \mathbf{v}} = 0 \tag{2.1.3}$$

2.1.2 Jeans equation

When we try to solve the CBE (2.1.1), the quantities described in it are virtually impossible to measure. The standard approach is then to integrate the CBE with respect to any quantity we can not observe. Even though we end up losing some information, we end up with an equation built on observables which we can handle.

We begin by taking the zero-th order momentum of the CBE. Recall that velocity does not explicitly depend on the position $\int v_i \frac{\partial f}{\partial x_i} d^3\mathbf{v} = \frac{\partial}{\partial x_i}\int v_i f d^3\mathbf{v}$:

$$\int \frac{df}{dt} d^3\mathbf{v} = 0 \Rightarrow \int \frac{\partial f}{\partial t} d^3\mathbf{v} + \frac{\partial}{\partial x_i}\int v_i f d^3\mathbf{v} - \frac{\partial \Phi}{\partial x_i}\int \frac{\partial f}{\partial v_i} d^3\mathbf{v} = 0 \tag{2.1.4}$$

We define now a probability density for the system, $\rho = f d^3\mathbf{v}$. The second term can be simplified if we introduce the mean particle velocity $\overline{v_i} = \frac{1}{\rho}\int f v_i d^3\mathbf{v}$ [3]. Recalling the divergence theorem (see appendix C.2), the last term becomes $\int f d^2 v$ which must be zero since it is not possible for any particle to have infinitely large velocities at boundaries[4].

$$\frac{\partial \rho}{\partial t} + \frac{\partial}{\partial x_i}\rho\bar{v_i} = 0 \tag{2.1.5}$$

[3] $\bar{X} = \frac{\int X f d^3\mathbf{v}}{\int f d^3\mathbf{v}}$.

[4] Nor outside boundaries for that matter.

This can be seen as the continuity equation in phase-space. Eq. (2.1.5) tells us that the probability density ρ is conserved so that dark matter particles can not be annihilated or created (if a particle disappears it is because it has moved away from the system).

We continue by taking the first momentum of CBE:

$$\int v_i \frac{df}{dt} d^3\mathbf{v} = 0 \Rightarrow \frac{\partial}{\partial t}\int v_j f d^3\mathbf{v} + \frac{\partial}{\partial x_i}\int v_j v_i f d^3\mathbf{v} - \frac{\partial \Phi}{\partial x_i}\int v_j \frac{\partial f}{\partial v_i} d^3\mathbf{v} = 0 \quad (2.1.6)$$

For the last term we can write the integral explicitly:

$$\int v_j \frac{\partial f}{\partial v_i} d^3\mathbf{v} = \int \frac{\partial (v_j f)}{\partial v_i} d^3\mathbf{v} - \int f \frac{\partial v_j}{\partial v_i} d^3\mathbf{v} = 0 - \delta_{ij}\rho \quad (2.1.7)$$

The other terms are the same as before and we are able to re-write eq.(2.1.6):

$$\frac{\partial}{\partial t}(\bar{v_j}\rho) + \frac{\partial}{\partial x_i}(\overline{v_i v_j}\rho) - \frac{\partial \Phi}{\partial x_j}\rho = 0 \quad (2.1.8)$$

Introducing the velocity-dispersion tensor $\sigma_{ij}^2 = \overline{v_i v_j} - \bar{v_i}\bar{v_j}$ and since we are assuming that the system is motionless on average, $\sigma_{ij}^2 = \overline{v_i v_j}$ (no bulk motion or flow). We then take the first momentum of the collisional continuity equation (2.1.5) and subtract it from eq.(2.1.8). This will lead us to the Jeans equations (they are three, one for each coordinate):

$$\frac{\partial \bar{v_j}}{\partial t} + \bar{v_i}\frac{\partial \bar{v_j}}{\partial x_i} = -\frac{1}{\rho}\frac{\partial (\rho \sigma_{ij}^2)}{\partial x_i} - \frac{\partial \Phi}{\partial x_j} \quad (2.1.9)$$

This equation derived in phase-space, is analogous to the Euler equation (2.2.7) that we will derive in the next section. We are left with an incomplete set of equations, have ten independent parameters[5] for only four equations (eqs. (2.1.3) and (2.1.9)). It is now a good idea to make some assumptions on our system, so that we end up with the same number of equations and independent components.

When in spherical coordinates (see app. (C.2)) we will simplify assuming that we have spherical symmetry: $\bar{v_\theta} = \bar{v_\phi} = 0$, that σ_{ij}^2 is diagonal: $\sigma_r^2 = \sigma_{rr}^2$, $\sigma_t^2 = \sigma_{\theta\theta}^2 = \sigma_{\phi\phi}^2$ and finally, that the system is steady ($\partial/\partial t = 0$).

From the Poisson equation, in spherical coordinates and assuming spherical symmetry, app. C.2:

$$4\pi G\rho = \nabla^2\Phi = \frac{1}{r^2}\frac{\partial}{\partial r}\left(r^2 \frac{\partial \Phi}{\partial r}\right) \Rightarrow \quad (2.1.10)$$

$$4\pi G \int \rho r^2 dr = r^2 \frac{\partial \Phi}{\partial r} \Leftrightarrow \quad (2.1.11)$$

$$\frac{GM}{r^2} = \frac{\partial \Phi}{\partial r} = -F_r \quad (2.1.12)$$

[5]Note that σ_{ij}^2 is symmetric.

With M the enclosed mass at radius r, we can write the Jeans' equation as:

$$-\frac{GM}{r} = \sigma_r^2 \frac{d\log(\rho\sigma_r^2)}{\partial r} + 2\beta \tag{2.1.13}$$

The quantity β is what we call the velocity anisotropy for dark matter (DM) and tells us how isotropic the distribution of particles is, giving us a relation between radial and transversal velocity: $\beta_{DM} = 1 - \frac{\sigma_t^2}{\sigma_r^2}$. To be physically valid, this quantity must be constrained: $-\infty < \beta_{DM} < 1$.

Solving the previous equation with respect to the mass:

$$M_{Jeans} = -\frac{r\sigma_r^2(r)}{G}\left(\frac{d\log\rho_{DM}}{d\log r} + \frac{d\log\sigma_r^2}{d\log r} + 2\beta_{DM}(r)\right) \tag{2.1.14}$$

When we derive the total mass from this equation, we will call it the "Jeans' mass". Later, we will compare this with the total mass derived when studying fluid dynamics.

2.2 Fluid Dynamics

Here we give the tools to describe fluid dynamics with reference to Landau [27]. This will allow us to describe the dynamics of the gas in the ICM.

We start by treating a fluid as a continuous medium which is valid if we consider a small volume element in the fluid when in comparison to the total volume of the body and, at the same time, large enough when in comparison to inter-particle distance. We will be neglecting processes of energy dissipation that may occur, such as viscosity, and will consider the fluid as ideal, hence incompressible, so that $\boldsymbol{\nabla}\cdot\mathbf{v} = 0$. In the end we will obtain the hydrostatic equilibrium equation that we will refer to several times.

2.2.1 Euler Equation

To describe the fluid dynamics we first need to consider the velocity of the fluid at coordinate (t, x, y, z) so that we can get to the equations of motion for the fluid. With the Lagrangian description we will take a certain path and see how the velocity[6] changes along that path.

$$d\mathbf{v} \equiv \frac{\partial\mathbf{v}}{\partial t}dt + \frac{\partial\mathbf{v}}{\partial x}dx + \frac{\partial\mathbf{v}}{\partial y}dy + \frac{\partial\mathbf{v}}{\partial z}dz \Rightarrow \frac{d\mathbf{v}}{dt} = \frac{\partial\mathbf{v}}{\partial t} + (\mathbf{v}\cdot\nabla)\mathbf{v} \tag{2.2.1}$$

Here, we can define the total derivative:

$$\frac{d}{dt} = \frac{\partial}{\partial t} + (\mathbf{v}\cdot\nabla) \tag{2.2.2}$$

[6]Velocity: $\mathbf{v} = \frac{d\mathbf{x}}{dt}$ in cartesian coordinates.

From mass conservation we can relate the rate of change of the total mass in a volume V_0 with the total mass flux through the infinitesimal surface area $d\mathbf{S}$. The total mass flux can be expressed in terms of volume recalling the divergence theorem $\oint \rho\mathbf{v} \cdot d\mathbf{S} = \int \boldsymbol{\nabla} \cdot (\rho\mathbf{v}) dV$

$$\frac{\partial}{\partial t} \int \rho dV = -\int \nabla \cdot (\rho\mathbf{v}) dV \Leftrightarrow \int \left[\frac{\partial \rho}{\partial t} + \nabla \cdot (\rho\mathbf{v}) \right] dV = 0 \tag{2.2.3}$$

Since we have set no constraints on the volume, eq.(2.2.3) must hold for any volume and the integrand must vanish (see here the similarities with the CBE 2.1.3).

$$\frac{\partial \rho}{\partial t} + \nabla \cdot (\rho\mathbf{v}) = 0 \tag{2.2.4}$$

Equation (2.2.4) is what we call the Continuity Equation and it must always be satisfied.

To get the force acting on some volume in the fluid, we integrate the force acting on a surface element $d\mathbf{A}$ over the surface of the fluid element:

$$\mathbf{F} = -\oint p d\mathbf{A} = -\int \nabla p dV \tag{2.2.5}$$

From Newton's law of inertia $\mathbf{F} = m\mathbf{a}$, we can relate it to (2.2.5) as the force acting on the fluid per unit of volume $\frac{d\mathbf{F}}{dV} = \frac{dm}{dV}\frac{d\mathbf{v}}{dt}$.

$$-\nabla p = \rho \frac{d\mathbf{v}}{dt} \tag{2.2.6}$$

Any external force acting on the fluid can be added in eq. (2.2.6). We assume that the fluid is subject to a gravitational field alone which adds a force term of $\mathbf{F} = -\boldsymbol{\nabla}\Phi$.

$$\frac{d\mathbf{v}}{dt} = \frac{\partial \mathbf{v}}{\partial t} + (\mathbf{v} \cdot \boldsymbol{\nabla})\mathbf{v} = -\frac{1}{\rho}\nabla p - \boldsymbol{\nabla}\Phi \tag{2.2.7}$$

This equation is known as the Euler equation and is the starting point for estimating the cluster's dynamical mass. The gas in the ICM can be well described in the ideal gas model and we write its equation of state as $p = \frac{k_B}{\mu m_p}\rho T$, where p is the pressure, k_B the Boltzmann constant, μ the mean atomic weight (which we assume to be 0.61), m_p the proton mass and T the temperature. Furthermore, we will make the wrong assumption that the gas is in static equilibrium, $\frac{d\mathbf{v}}{dt} = 0$.

Assuming spherical symmetry we can write the Euler equation in spherical coordinates (see app. C.2) and considering the Poisson equation in spherical coordinates (eq.(2.1.12)), the Euler equation can be easily solved in order to obtain the mass inside a sphere of radius r:

$$-\frac{1}{\rho(r)}\frac{d}{dr}\frac{\rho k_B T}{\mu m_p}\hat{e}_r = \frac{GM}{r^2}\hat{e}_r \Leftrightarrow \tag{2.2.8}$$

$$\Leftrightarrow M_{HE}(r) = -rT(r)\frac{k_B}{G\mu m_p}\left(\frac{d\log\rho}{d\log r} + \frac{d\log T}{d\log r}\right) \tag{2.2.9}$$

Equation (2.2.9), is called the hydrostatic equilibrium equation. In cluster dynamics this is the simplest way for estimating its mass from the gas density and temperature radial profile that can be obtained when analysing X-ray spectra as discussed in introduction. When estimating the cluster total mass under this assumption, we will call it the "hydrostatic mass".

2.3 Comparing collisional and collisionless to determine the cluster's mass

Here we write the hydrostatic equilibrium equation and the Jeans' equation, derived in this chapter. For the gas we assumed the systems to be spherical and in hydrostatic equilibrium::

$$M_{HE}(r) = -rT(r)\frac{k_B}{G\mu m_p}\left(\frac{d\log\rho}{d\log r} + \frac{d\log T}{d\log r}\right) \tag{2.3.1}$$

For the dark matter, we assumed the system to be also spherical and motionless on average. This lead us to the Jeans' equation:

$$M_{Jeans} = -\frac{r\sigma_r^2(r)}{G}\left(\frac{d\log\rho_{DM}}{d\log r} + \frac{d\log\sigma_r^2}{d\log r} + 2\beta_{DM}(r)\right) \tag{2.3.2}$$

Comparing these two different equations, derived for two different systems, one collisional (gas) and the other collisionless (DM). They both give us the total mass of the cluster[7], therefore we can equate both, $\mathrm{M}_{HE}(r) = \mathrm{M}_{Jeans}(r)$:

$$T_g\frac{k_B}{\mu m_p}\left(\frac{d\log\rho_g}{d\log r} + \frac{d\log T_g}{d\log r}\right) = \sigma_r^2\left(\frac{d\log\rho_{dm}}{d\log r} + \frac{d\log\sigma_r^2}{d\log r} + 2\beta\right) \tag{2.3.3}$$

From X-ray observations we have access to all quantities needed to describe the left-hand side (LHS), that is the gas temperature and density profiles, necessary to solve the hydrostatic equilibrium equation. For the right-hand side (RHS) however, we are less fortunate. It is still not possible to measure any dark matter directly. Nevertheless, we know that the cluster's gravitational mass is the sum of all particles comprising the cluster. Neglecting stars and dust, we can estimate the dark matter density distribution: $\rho_{DM}(r) = \rho_{Total}(r) - \rho_g(r)$, where ρ_{Total} is the density of the cluster from eq.(2.2.9) [8].

[7] This is only correct to say if the assumptions so far made, are also correct.

[8] The density can be calculated from the total mass assuming spherical symmetry (see eq.(A.1.7)). For now, we are assuming $M_{Total}(r) = M_{HE}(r)$.

We continue relating the gas with dark matter quantities. Note that, if we take the Jeans equation (2.1.14) and say that the velocity dispersion tensor is isotropic ($\beta = 0$) this equation gets reduced to the hydrostatic equilibrium equation (2.2.9). The effective dark matter temperature[9] is defined as a function of two parameters for dark matter: radial dispersion velocity (σ_r) and velocity anisotropy ($\beta_{DM} \equiv 1 - \frac{\sigma_t^2}{\sigma_r^2}$), see app.A.1, where we write the temperature as:

$$T_{DM} = \frac{\mu m_p}{k_B}\sigma_r^2\left(1 - \frac{2}{3}\beta_{DM}\right) \tag{2.3.4}$$

We can then assume that the dark matter temperature and the gas temperature are the same ($T_g(r) \sim T_{DM}$), as it was proven to be true from numerical simulations [23] so that eq.(2.3.4) can then be inverted, in order to give us the velocity dispersion:

$$\sigma_r^2 = \left[\frac{\mu m_p}{k_B}\left(1 - \frac{2}{3}\beta_{DM}\right)\right]^{-1} T_g \tag{2.3.5}$$

Note, that we are still left with one free-parameter, β_{DM}, which to be physically valid must be constrained: $-\infty < \beta_{DM} < 1$. For an isotropic velocity distribution, $\beta = 0$ and for a radial biased velocity dispersion: $0 < \beta < 1$.

2.3.1 The data for the gas

To study the cluster's dynamics we will be needing reliable data for the gas as if we had it from X-ray observations. Hence, we will need the gas density and temperature measurements at different radii.

We will first use this "fake" (but reliable) data to estimate the cluster's total mass assuming hydrostatic equilibrium. However, there could be a contribution of the gas velocity, and pressure from magnetic fields and cosmic rays present in the ICM, which are not given by X-ray measurements. These three different contributions will have to be taken into account when estimating the cluster's total mass, and will be discussed in further detail.

To simulate such data we assume that we have access to the dark matter particles in the cluster, in particular to the properties needed to estimate the Jeans' mass from the Jeans' eq. (2.1.14), ρ_{DM}, σ_r^2 and β_{DM}. We assume that ρ_{DM} follows the NFW model (eq.(1.1.1)) and for simplicity $\beta_{DM} = 0$. In app. A.2 we give the details on how we obtain the gas density and temperature, given the dynamics of dark matter particles in a cluster.

To be true to observations we choose typical values for the gas central value $\rho_g(r_0) = 10^3$ cm^{-3} and $a = 500$ kpc [37]. From Vikhlinin et al. [40] we took as typical value $R_{200} = 1.8$ Mpc. Note that typically, X-ray observations span $\sim 10 - 1000$ kpc, only two orders of magnitude whereas here we take a larger sample. Thus,

[9]Dark matter is collisionless, therefore the temperature for dark matter is not defined as if it was in thermodynamic equilibrium.

whenever we want to relate to what we can actually observe from X-rays, we should consider the central area of the graphics $[0.01, 1]$ R_{200}.

The comparison between the dynamics of a collision and collisionless system will appear again in chapter 4.1, with a different purpose than to simulate "fake" data for the gas from X-ray observations.

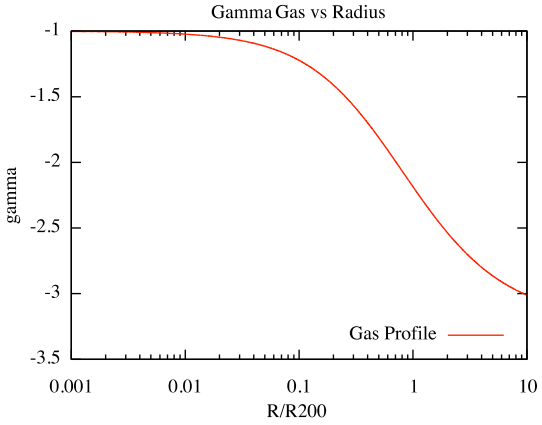

(a) Density profile

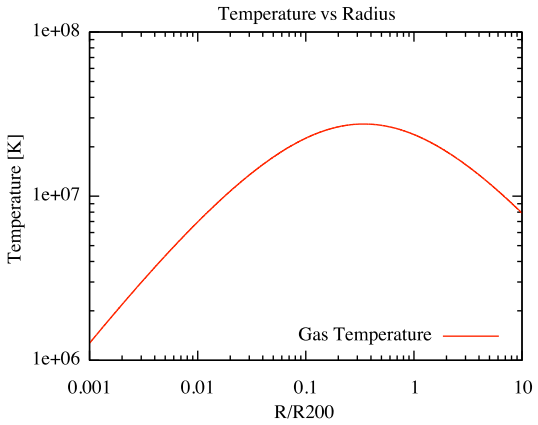

(b) Total mass of the cluster assuming hydrostatic equilibrium

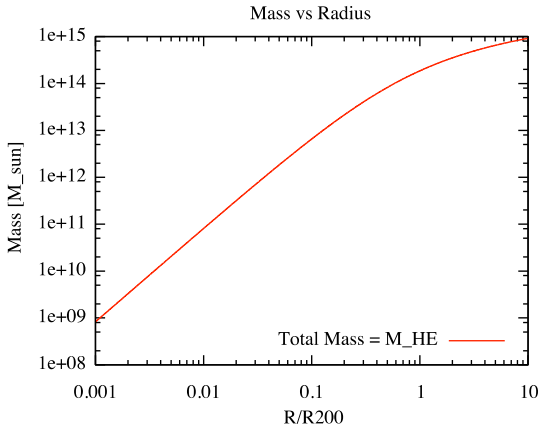

(c) Total mass of the cluster assuming hydrostatic equilibrium

Figure 2.3.1: "Fake" data for the gas fitted within the sample $[0.001, 10]R_{200}$. Fig. 2.3.1a shows the gas density profile, $\gamma_g = \frac{d \log \rho_g}{d \log r}$, it follows the NFW model. The density profile is fitted to a double power-law with $\rho_g(r_0) = 10^3$ cm^{-3} and $a = 500$ kpc. Fig. 2.3.1b the temperature profile obtained from eq.(A.1.13). From the temperature and density we calculate the total mass (fig. 2.3.1c) assuming the gas to be in hydrostatic equilibrium, eq. (2.2.9). See app. A.2 for the details on how to get such properties for the gas.

Chapter 3

Beyond the hydrostatic mass calculus

In the previous section, while deriving the hydrostatic equilibrium equation (2.2.9) we assumed that the fluid was spherical and in static equilibrium. This was a fairly simplified model of the gas' dynamics, as we have ignored the gas velocity in Euler's equation and other pressure effects.

We will recast Euler's equation (2.2.7) and proceed with the full description for the dynamics of the the cluster. We will not neglect the velocity of the gas and see how this will be different from the hydrostatic equilibrium equation (2.2.9).

Furthermore, we have seen that any external force acting on the fluid can also be added in this equation (2.2.7). We will be discussing the influence of magnetic fields and cosmic rays present in galaxy clusters. We define the term non-thermal pressure (when referring to the non-thermal gas motion, magnetic fields and cosmic rays) to distinguish from the pressure exerted by thermal electrons, P_g.

3.1 Non static fluid

3.1.1 Euler equation

We have previously derived Euler's equation in its most general form (2.2.7). We consider only its radial component since we are still assuming spherical symmetry. Here we re-write it as:

$$\frac{\partial v_r}{\partial t} + (\mathbf{v} \cdot \boldsymbol{\nabla})\, v_r = -\frac{1}{\rho}\nabla_r p - \nabla_r \Phi \tag{3.1.1}$$

The RHS of this equation should be familiar to us by now and on the LHS we have the acceleration. With the tools derived in app. (C.2), this equation can be explicitly written:

$$\dot{v_r} - \frac{v_\theta^2 + v_\phi^2}{r} + \left(v_r \frac{\partial}{\partial r} + \frac{v_\theta}{r \sin\phi} \frac{\partial}{\partial \theta} + \frac{v_\phi}{r} \frac{\partial}{\partial \phi} \right) v_r = -\frac{1}{\rho} \nabla_r p - \nabla_r \Phi \Leftrightarrow$$

$$M_{Total}(r) = M_{HE}(r) - \frac{r^2}{G} \dot{v_r} + \frac{r}{G} \left(v_\theta^2 + v_\phi^2 \right) - \frac{r^2 v_r}{G} \frac{\partial v_r}{\partial r} - \frac{r v_\theta}{G \sin\phi} \frac{\partial v_r}{\partial \theta} - \frac{r v_\phi}{G} \frac{\partial v_r}{\partial \phi}$$

We define M_{HE} to be the cluster's mass estimated under the assumption of the gas in the ICM being in hydrostatic equilibrium, see eq. (2.2.9). M_{Total} in this case, is the cluster total mass estimated under the assumption of a non-static fluid, which can be different from the hydrostatic mass.

We assume that there is no acceleration or that the velocity changes slowly in time, allowing us to ignore $\dot{v_r} = dv_r/dt \sim 0$. Overall, we are considering that the radial velocity does not have any angular dependence, which lead us to ignore the last two terms:

$$M_{Total}(r) = M_{HE}(r) + \frac{r}{G} \left(v_\theta^2 + v_\phi^2 - r v_r \frac{dv_r}{dr} \right) \tag{3.1.2}$$

We define the extra mass term: $\Delta\mathrm{M}(r) = \frac{r}{G} \left(v_\theta^2 + v_\phi^2 - r v_r \frac{dv_r}{dr} \right)$. The presence of this term will introduce a bias on the total mass estimations, when assuming hydrostatic equilibrium [1]. Neglecting this bias will not only give us the wrong total mass, but also the wrong dark matter mass profile [2].

We see that the presence of bulk rotation $(v_\theta^2 + v_\phi^2)$ will add more mass into the total mass estimation as this term is always positive. The effect of radial bulk motion (v_r) can go either way [3] depending on its velocity distribution.

3.1.2 Effect of velocity

To get an idea how the motion of the gas affects the mass estimation we need to know roughly the order of magnitude of these velocities and how it describes different cluster dynamics. Measuring these velocities in a galaxy cluster has proven to be very difficult, for technical details go to app. B.4. Brunetti et al. [9], show that we can have bulk motion (v_r) of the order of $10^2 - 10^3 \mathrm{km \cdot s^{-1}}$, [4] at the virial radius in massive clusters, due to cluster mergers and accretion. They do this with numerical simulations. For a cluster with $M = 10^{14} M_\odot$ its circular velocity at the virial radius its typically $10^3 \mathrm{km \cdot s^{-1}}$, [5].

We will take as an example, a cluster with no bulk rotation and that is not undergoing any merger. In this way, we consider that the gas is infalling $(v_r < 0)$ in the cluster's outskirt. We consider the case of outflow in the cluster's core $(v_r > 0)$,

[1] So far, we have been saying that in the hydrostatic equilibrium equation, $\mathrm{M}_{HE}(r) = \mathrm{M}_{Total}(r)$.
[2] $M_{DM}(r) = M_{Total}(r) - M_g(r)$.
[3] "Adding" or "subtracting" dynamical mass.
[4] Tangential velocity of the Sun around the Galaxy $\sim 200 \mathrm{km \cdot s^{-1}}$.
[5] $v_c(r_{vir}) = \sqrt{GM(r_{vir})/r_{vir}}$

this may happen due to the presence of AGNs, a recent supernovae explosion, a gamma ray burst or some other phenomena that may heat the gas and expel matter.

The velocity profile adopted can be seen in Fig.3.1.1 (left). Note that in the trivial case of considering no relative motion of the gas, there is no bias introduced. Between the cluster's outskirts and its centre we assume the gas to be motionless on average.

The effect that ΔM will have on total mass estimation can be seen as a bias effect in the same figure (right). We define this bias in percentage:

$$b(r)_{[\%]} = \frac{M_{HE}(r) - M_{Total}(r)}{M_{Total}(r)} \times 100 \tag{3.1.3}$$

$$b(r)_{[\%]} = -\frac{\Delta M(r)}{M_{Total}(r)} \times 100 \tag{3.1.4}$$

The results obtained with such a model are as shown in Fig. 3.1.1, due to our choice of the velocity profile, we have $\Delta M \geq 0$ which makes the bias always negative, hence the total mass is underestimated if we consider hydrostatic equilibrium.

We could have also considered the gas to be infalling towards the center of the cluster. In that case this would mean $v_r \frac{dv_r}{dr} < 0$, which would have a positive contribution to the mass estimation ($\Delta M > 0$), and would also cause a negative bias in the centre. The infall of the gas in the centre of clusters happens for clusters with short cooling times. The gas in the centre will become highly dense and cool due to radiative mechanisms and in the absence of heating mechanisms, the gas will have to flow in to maintain hydrostatic equilibrium, this is also known as cooling flow.

Furthermore, if the gas velocity is $v_r^2 \sim v_{vir}^2 \sim 10^3$ km·s^{-1}, the contribution on the cluster's total mass from ΔM will be almost the same as M_{HE}:

$$\Delta M = 1/G(r v_r^2) \sim 0.5 M_{HE}$$

Corresponding to a change in the bias to approximately 50%.

What people have been doing so far is to neglect the gas' velocity in the Euler equation. Moreover, even when knowing that the gas' velocity should introduce some bias, they have done it wrong as it was done by Lagana et al. [26] by taking some sort of isotropic turbulent pressure $P_{turb} = 1/3\rho_g(\sigma_r^2 + \sigma_t^2)$ which adds into Euler equation as an extra pressure term. This should not be the case as the Euler equation, as we have written in (3.1.1), fully describes the gas' motion in the ICM and there is no need of such assumptions.

3.2 Extra pressure support

To continue with the full description of the gas motion in the ICM we consider other extra-pressure terms present in the ICM that along with the gas pressure, balance gravitation. For simplicity, we will neglect the velocity terms, that we can just

sum up in the end into our equations. When assuming static equilibrium, Euler's equation can be written as

$$\frac{1}{\rho}\nabla p = \boldsymbol{\nabla}\Phi \tag{3.2.1}$$

Other extra pressure terms that may be present will add a contribution: $p = P_g + P_{extra}$, where P_g is simply the pressure from the gas. As usual, we will assume spherical symmetry and the previous equation can be re-written as:

$$\frac{1}{\rho_g(r)}\frac{dp}{dr} = -\frac{d\Phi}{dr} \Leftrightarrow \tag{3.2.2}$$

$$-\frac{1}{\rho_g(r)}\frac{d(P_g + P_{extra})}{dr} = \frac{GM_{Total}(r)}{r^2} \Leftrightarrow \tag{3.2.3}$$

$$M_{Total}(r) = -\frac{r^2}{G\rho_g(r)}\frac{d}{dr}\frac{\rho k_B T_g}{\mu m_p} - \frac{r^2}{G\rho_g(r)}\frac{dP_{extra}}{dr} \Leftrightarrow \tag{3.2.4}$$

$$M_{Total}(r) = M_{HE}(r) - \frac{r^2}{G\rho_g(r)}\frac{dP_{extra}}{dr} \tag{3.2.5}$$

What people have been trying to do is to take observational measurements (these can not be from X-rays) of this extra-pressure which may come from the presence of magnetic fields and cosmic rays, and add them in the hydrostatic mass, estimated with X-ray observations. As an example take, [26].

3.2.1 Magnetic pressure

To study how the magnetic field acting back on the plasma contributes to the gas pressure support, we introduce Lorenz force as an extra external force term [8, pp. 58] .

$$\rho\mathbf{F} = \mathbf{j} \times \mathbf{B} \tag{3.2.6}$$

The current density $\mathbf{j}$, is given by Ampère's law $\mathbf{j} = \frac{1}{\mu_0}(\nabla \times \mathbf{B})$, with μ_0 the magnetic constant [6] and $\mathbf{B}$ the magnetic field.

Adopting the vector identity $\nabla\left(\frac{1}{2}\mathbf{B}\cdot\mathbf{B}\right) = \mathbf{B}\times(\nabla\times\mathbf{B}) + (\mathbf{B}\cdot\nabla)\,\mathbf{B}$

$$\rho\frac{d\mathbf{v}}{dt} = \rho\nabla\Phi - \nabla p + \rho\mathbf{F} = \left[-\frac{\nabla B^2}{2\mu_0} + \frac{1}{\mu_0}(\mathbf{B}\cdot\nabla)\,\mathbf{B}\right] \tag{3.2.7}$$

where $\frac{B^2}{2\mu_0}$ can be defined as the magnetic pressure and the second term inside the square bracket represents a tension force that is different from zero if the magnetic field is curved [8, pp. 83].

When substituting this new pressure term into eq. (3.2.5), we end up with the magnetic hydrostatic equation

[6] $\mu_0 = 4\pi \times 10^{-7}$ NA^{-1} in SI units.

$$M_{Total}(r) = M_{HE} - \frac{r^2}{\rho_g(r)G}\frac{1}{2\mu_0}\frac{d\left\langle B^2(r)\right\rangle}{dr} \tag{3.2.8}$$

From observations of galaxy clusters and several magneto-hydrodynamics simulations, we expect observations of the magnetic field to decrease with distance to the centre meaning that $\frac{dB^2(r)}{dr} < 0$ [6]. This is in agreement with the theory that tell us that this fields could be seeded amplified in the cluster's center due to astrophysics phenomena.

Note that if we neglect the extra term in eq.(3.2.8) considering only hydrostatic equilibrium we expect that the total mass estimation of the cluster will be underestimated. To see this, note that $\frac{r^2}{\rho_g(r)G}\frac{1}{2\mu_0}\frac{d\left\langle B^2(r)\right\rangle}{dr} < 0$. Therefore, it is expected that the magnetic pressure should be more significant close to the cluster's centre than close to the virial radius.

To know how much bias we have when neglecting magnetic pressure, we took the same magnetic profile as the one in [6] derived from radio observations of the Coma cluster, assuming the magnetic field to be constant at each radius.

$$\langle B(r)\rangle = \langle B_0\rangle \left(\frac{\rho_g(r)}{\rho_{g0}}\right)^{\Psi} \tag{3.2.9}$$

We changed the central value B_0 to typical values for NCC and CC cluster which are estimated to be on the order of $2 - 30\mu$G, respectively [26], and at the same time we also changed Ψ for each choice of B_0. We show the results, again in terms of how much bias $b(r)$ (3.1.4), can be introduced due to the presence of magnetic fields. We considered two different ranges for the shape parameter, in fig. 4.1.4a and fig.3.2.1b.

From Fig.3.2.1 we see the effect that the magnetic field has on the cluster's mass estimation.

Here we see what was already expected, that the bias in the cluster's mass estimation is more significant closer to the center. At the virial radius, the bias introduced can be negligible for weak magnetic fields or account up[7] to -30% when we have strong magnetic fields ($\sim 20\mu$G).

Of course these results can be argued. Due to the chaotic nature of the magnetic field in the ICM, we should not expect such a nice behaviour as the one modelled in (3.2.9). Nevertheless, this model illustrates well that the intensity of magnetic fields decrease as we go further out from the cluster's centre. This seems reasonable, since we are not expecting that the magnetic field can be amplified at large distance from the cluster's centre. This study then shows, that close to the virial radius we can have a bias on total mass estimation from X-rays under the assumption of hydrostatic equilibrium from -1% up to -30%.

[7]The word "up" is used to mention the bias in modulus, as in the overall effect that the non-thermal pressure has in the total dynamical mass.

3.2.2 Cosmic Rays pressure

The pressure effect that cosmic rays have on the cluster is not totally clear as observations are still poor. Even though it is not possible to set a real constraint on this pressure, one way to study its contribution is to define a ratio between the pressure from cosmic rays (CRs) and gas $Y_p(r) \equiv \frac{P_{CRs}(r)}{P_g(r)} \Leftrightarrow P_{CRs}(r) = P_g(r)Y_p(r)$. From Euler's equation (3.2.5) we now have:

$$M_{Total}(r) = M_{HE} - \frac{r^2}{G\rho_g(r)}\frac{d(P_g Y_p)}{dr} \Leftrightarrow \tag{3.2.10}$$

$$M_{Total}(r) = M_{HE} - \frac{r^2}{G\rho_g(r)}Y_p(r)\frac{d(P_g)}{dr} - \frac{r^2}{G\rho_g(r)}P_g(r)\frac{d(Y_p)}{dr} \Leftrightarrow \tag{3.2.11}$$

$$M_{Total}(r) = M_{HE} + Y_p(r)M_{HE} - rT(r)Y_p(r)\frac{k_B}{\mu m_p G}\frac{d\log Y_p}{d\log r} \tag{3.2.12}$$

In general there should be a dependence of cosmic ray's pressure with the radius but since we know nothing about this, let us parametrize $Y_p(r)$ with a simple power-law as it was done in Ando et al.[1]:

$$Y_p(r) = Y_{p0}\left(\frac{r}{r_0}\right)^{\beta_{cr}} \tag{3.2.13}$$

With a wide range of values adopted for the Y_{p0} ratio at cluster center and β a shape parameter, we could study the bias introduced by cosmic rays into the calculus of the cluster mass only from X-ray observations assuming hydrostatic equilibrium. We take these values to be $0.1 < Y_{p0} < 0.5$ and $-0.3 < \beta_{cr} < -0.7$, which makes a positive contribution on Δ M: $\mathrm{M}_{Total}(r) = \mathrm{M}_{HE}(r) + \Delta\ \mathrm{M}(r)$, since this parametrisation translates into an effect of cosmic rays closer to the cluster's center. As discussed in the introduction, cosmic rays can be created by shocks and AGN which are not expected to be present in the cluster's outskirts. Furthermore, there must be a correlation between magnetic fields and cosmic rays and we have just seen that this has a bigger contribution in the cluster's centre.

As expected from the correlation between cosmic rays and magnetic fields, their effect on the mass profile is very similar. What this means is that if we have access to the information about $\Delta\mathrm{M}(r)$, this is degenerate as we are not able to distinguish $\Delta\mathrm{M}_B(r)$ and $\Delta\mathrm{M}_{cr}(r)$ apart. To remove this degeneracy we would have to rely on other observational methods, see app.B.3. Nevertheless, having access to $\Delta\mathrm{M}(r)$ could give us some insight on how things may be behaving in the ICM.

3.3 Overall

Considering all the three different contributions into Euler's equation, we get the full description for the dynamics in the cluster. Here we write all the terms explicitly, with $M_{HE}(r)$ being the hydrostatic equilibrium mass (recall eq.(2.2.9)):

$$M_{Total}(r) = M_{HE}(r) \tag{3.3.1}$$

$$+\frac{r}{G}\left(v_\theta^2 + v_\phi^2\right) - \frac{r^2 v_r}{G}\frac{dv_r}{dr} \tag{3.3.2}$$

$$-\frac{r^2}{\rho_g(r)G}\frac{1}{2\mu_0}\frac{dB^2(r)}{dr} \tag{3.3.3}$$

$$+Y_p(r)M_{HE}(r) - r^2 T_g(r)\left(\frac{k_B}{\mu m_p G}\right)\frac{dY_p}{dr} \tag{3.3.4}$$

Fig. 3.3.1 shows us how much contribution we could expect from combining the previous models for the velocity, magnetic fields and cosmic rays combined (second, third and fourth term in eq. (3.3.4)). As before, we show their contribution to the cluster's total mass by relating the cluster's true dynamical mass with a bias if we were to consider that $M_{Total}(r) = M_{HE}(r)$.

We should keep in mind that this bias profile is related to our choice in the profile chosen for the three different contributions to the cluster's total mass. The velocity of the gas can contribute positively or negatively. Our choice made this a positive contribution, which translates in an overall bias, close to the virial radius, of approximately -20 to -50%. Overall, the real minimum that we should be considering is the trivial one where bias is zero, that is the case of a cluster to be in hydrostatic equilibrium.

With this, we see that if the theoretical framework presented here is correct, we should expect to measure some bias in the cluster's total mass, when the assumption of hydrostatic equilibrium does not completely describe the dynamics of the gas in the ICM. For this reason, we know that with today's total mass estimations from X-rays alone, which is calculated at the virial radius with the hydrostatic equilibrium equation, we are driven into an over- or under-estimate on the cluster's true dynamical mass. The dynamical mass needs to be equal to the gravitational mass, and the latter is simply the sum of all particle's mass.

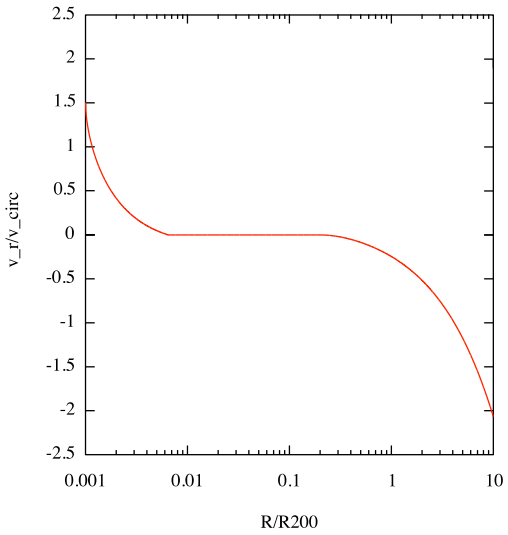

(a) Radial velocity

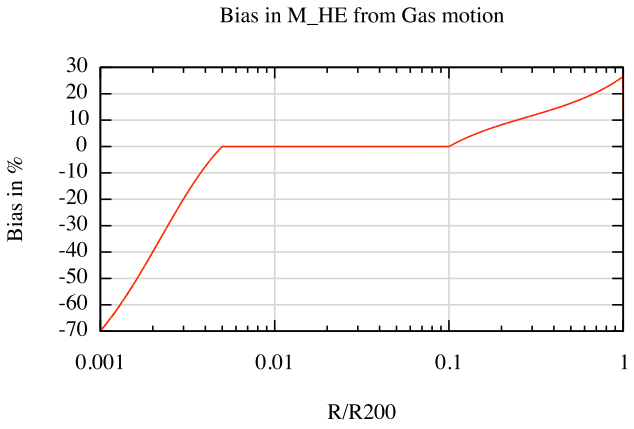

(b) $-v_r \frac{dv_r}{dr}$

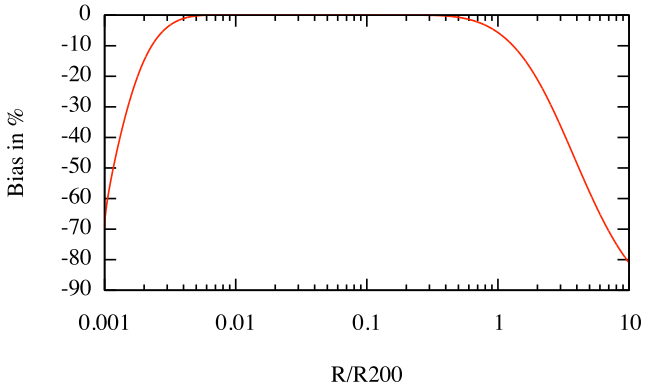

(c) $v_\theta^2 + v_\phi^2 - v_r \frac{dv_r}{dr}$

Figure 3.1.1: On top, the radial velocity profile with respect to the circular velocity ($v_c(r) = \sqrt{GM(r)/r}$). On the bottom, mass bias in % (see eq.(3.1.4)): on the left a picture showing that the influence of infall of the gas at the cluster's outskirts that gives a negative contribution to the total mass, and on the right, the influence of bulk motion and rotation which in this case, turns out to give a positive contribution in mass. We see that close to the virial radius (R_{200}) there will be a significant underestimation of 10% when neglecting this effect in total mass estimations. At the centre of the cluster this effect is not negligible if the gas particles have velocities of the order of $10^2 - 10^3$km s^{-1}, however, these values can be overestimated, which would correspond to less bias in the cluster's centre. Here we are considering that the cluster is not relaxed in its outskirts as there was not enough time for energy dissipation to occur from collision of gas' particles. We considered $v_r \sim 10^4$ km·s^{-1} at the virial radius. If we had considered one order of magnitude less, underestimation on the mass calculus would be $\sim 1\%$ instead of 10%.

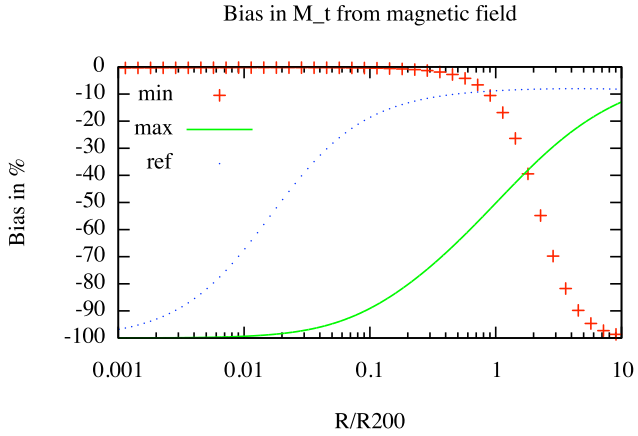

(a) $0.1 < \Psi < 0.9$

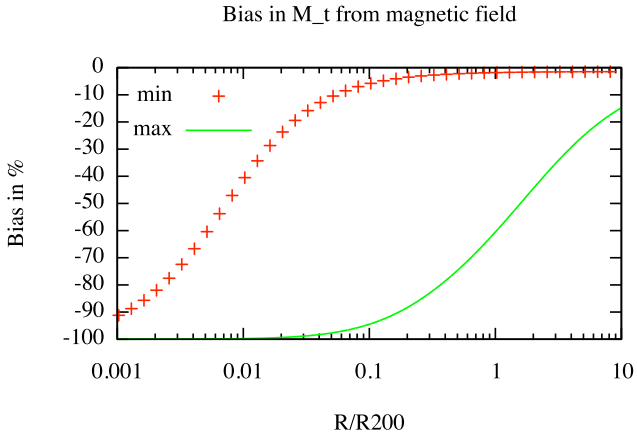

(b) $0.5 < \Psi < 0.9$

Figure 3.2.1: Mass bias in % vs R/R_{200}. On the left, we have taken a broad range of values for the parameters B_0 and Ψ in eq.(3.2.9) and calculate the bias in the total mass when neglecting magnetic pressure. We have found that under the model assumed for the magnetic field, $(\langle B_0 \rangle, \Psi) = (24.4\mu\text{G}, 0.74)$ maximised the overall contribution until the virial radius and $(\langle B_0 \rangle, \Psi) = (2.0\mu\text{G}, 0.1)$ minimises. For reference we have $(\langle B_0 \rangle, \Psi)_{ref} = (4.8\mu\text{G}, 0.6)$. We observed that for a choice in $\Psi < 0.5$ the bias in mass increases (is more negative) as the we get further out in the cluster, which does not seem reasonable. On the right, we considered as lower limit $\Psi = 0.5$, which agrees from observations by Dolag et al.[14]. Here we account for a minimum underestimation in mass as low as 1%, or even less close to the virial radius, up to -50%. There could also be the case that the intensity of the magnetic field in the cluster is even weaker than from what we have assumed, which could make this bias almost negligible.

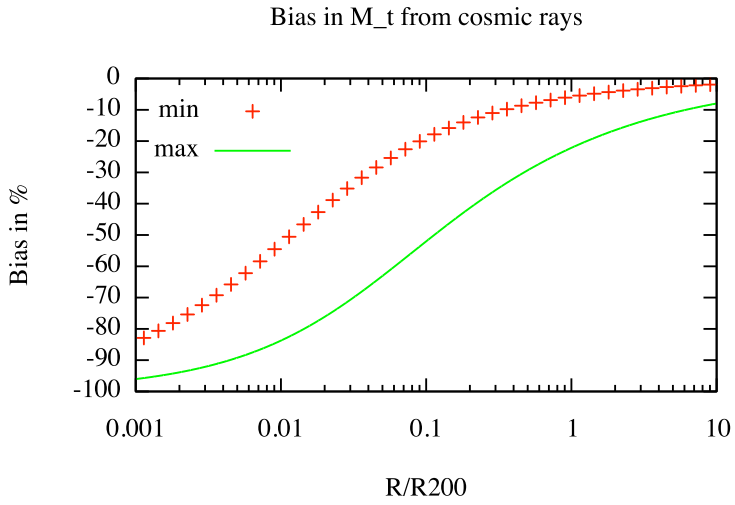

Figure 3.2.2: Mass bias in % vs R/R_{200}. When we calculate the total mass of a cluster considering the simplest case of spherical hydrostatic equilibrium this value is biased if we do not consider cosmic ray pressure. In this figure we see how much this is biased with the assumed model for the pressure exerted by cosmic rays. At the virial radius we have that if we ignore the pressure from cosmic rays, total mass estimations can be underestimated from a few% up to 30%. This is of the order of 50-80% in the central part of the cluster. Remember that if we are to compare with the hydrostatic equilibrium mass estimated X-ray observations, we should only consider the radial range [0.01, 1] R_{200}.

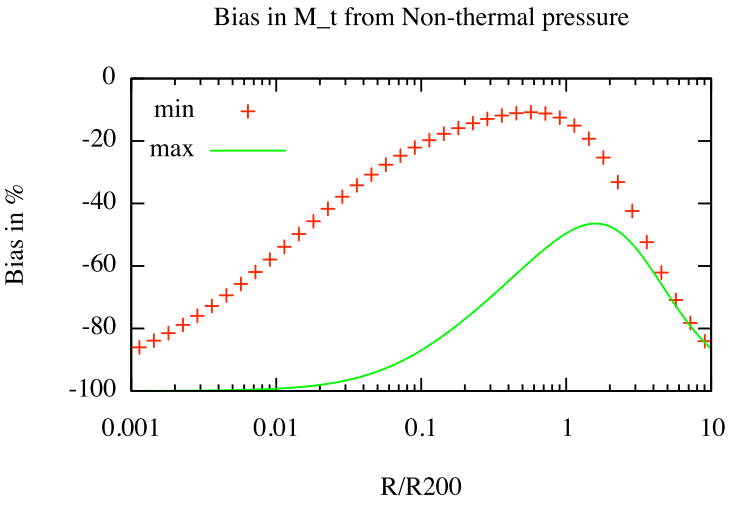

Figure 3.3.1: Mass bias in % vs R/R200. Considering the contribution from cosmic rays, magnetic field and the gas' velocity. We take the previous model for the radial velocity of the gas, plus the turbulence. As for the magnetic field we take $(\langle B_0 \rangle, \Psi)_{min}$ = (2.0μG,0.5) and $(\langle B_0 \rangle, \Psi)_{max}$ = (24.0μG,0.7), and for cosmic rays $(Y_{p0}, \beta_{cr})_{min}$ = (0.1,-0.5) and $(Y_{p0}, \beta_{cr})_{max}$ = (0.5,-0.5). We see that under these assumptions the overall hydrostatic mass estimation is at least 10% underestimated and at most it can have the same weight as hydrostatic mass hence, representing 50% of bias in the total mass.

Chapter 4

A new method to estimate the cluster's total mass

From observations of galaxy clusters in the X-rays spectral band, we have access to the gas' density and temperature profiles. Assuming the gas in the ICM to be in hydrostatic equilibrium and spherically distributed, the hydrostatic mass can be calculated (with the hydrostatic equilibrium eq. (2.2.9)).

Usually one assumes that the hydrostatic mass is the total mass of the cluster, since the dynamical mass and the gravitational mass are just two different ways to get to the same physical result. The gravitational mass M is simply the sum of the mass of the N particles inside the cluster:

$$M = \sum_{i}^{N} m_i$$

In the previous chapter we showed the consequences of the gas not being static, and what would happen to the dynamics if we also had a non-negligible contribution of magnetic fields and cosmic rays to the pressure in the ICM. In such conditions, we no longer can assume the cluster to be in hydrostatic equilibrium. For this reason the dynamical mass could not be given by the hydrostatic mass. We argued that it is possible for the dynamical mass to increase (or decrease) by a half of the hydrostatic mass: $\mathrm{M}_{Total}(r) = \mathrm{M}_{HE}(r) + \Delta\mathrm{M}(r)$, with $\Delta\mathrm{M}(r) \gtrless 0$.

In this chapter, our goal is to derive a method that give us the total mass of a cluster from X-ray measurements, without the usual assumption that the gas in the ICM is in hydrostatic equilibrium.

4.1 The method

To derive this method we start with the "fake" data for the gas, as if they came from X-ray observations, as we did for the previous chapter. We will later apply the method to a real cluster on the attempt of extracting $\Delta M(r)$ if the condition of hydrostatic equilibrium is not verified.

4.1.1 First assume hydrostatic equilibrium

From X-ray observations we can measure the gas density and temperature of the gas in the ICM. Assuming the distribution of the gas to be spherical and in hydrostatic equilibrium, we can calculate the hydrostatic mass from the hydrostatic equilibrium equation:

$$M_{HE}(r) = -rT(r)\frac{k_B}{G\mu m_p}\left(\frac{d\log\rho}{d\log r} + \frac{d\log T}{d\log r}\right) \tag{4.1.1}$$

When the cluster is in hydrostatic equilibrium, eq. (4.1.1) is the total mass of the cluster which we call the hydrostatic mass. Hence, $\mathrm{M}_{HE}(r) = \mathrm{M}_{Total}(r)$.

To estimate the total mass of the cluster without relying on the assumption of hydrostatic equilibrium, we will compare different ways to calculate the total mass, from X-rays measurements alone.

In section 2.1, we derived the Jeans' equation (4.1.2). We simplified the dynamics of the dark matter ensemble by saying that it is motionless on average, spherical symmetric and static. In this case, we have called this mass the Jeans' mass and $\mathrm{M}_{Jeans}(r) = \mathrm{M}_{Total}(r)$.

$$M_{Jeans}(r) = -\frac{r\sigma_r^2(r)}{G}\left(\frac{d\log\rho_{dm}}{d\log r} + \frac{d\log\sigma_r^2}{d\log r} + 2\beta(r)\right) \tag{4.1.2}$$

From observations, we are still not able to make direct measurements of dark matter particles. Nevertheless, we have some insight on the Jeans' equation by indirect analysis, and from numerical simulations. The parameters needed to calculate the Jeans' mass are the velocity dispersion for the dark matter, $\sigma_r^2(r)$, the gradient of its density, $\gamma_{DM}(r) = \frac{d\log\rho_{DM}}{d\log r}$ and the velocity anistropy profile, $\beta(r)$.

We make the pivotal assumption that the temperature of dark matter and the gas are the same [23], and that the temperature of the dark matter is related to the velocity dispersion. We will make assumptions on the velocity anisotropy profile, which from numerical simulations [20], we take $-1/2 < \beta_{DM}(r) < 1/2$. The density of dark matter will be calculated from the gravitational mass assuming that only the gas and dark matter particles contribute to it. From observations of galaxy clusters, we know that is an excellent assumption: $\mathrm{M}_{DM}(r) = \mathrm{M}_{Total}(r) - \mathrm{M}_g(r)$.

In the case of the gas and the dark matter being in hydrostatic equilibrium, both the hydrostatic and the Jeans' mass give, individually, the cluster's total mass. Therefore, it is expected that they should be equal to each other: $\mathrm{M}_{HE}(r) = \mathrm{M}_{Jeans}(r)$. On the other hand, if the previous condition turns out to be false, it means that we have made the wrong assumptions on the cluster's dynamical state. The wrong assumption could come either from the gas or the dark matter.

To show numerically the agreement between these two functions (M_{HE} and M_{Jeans}), we used the reduced χ^2 as a test [36], where σ_M^2 are the uncertainties:

$$\chi^2 = \frac{1}{N}\sum_i^N \frac{\left(M_{HE}(r_i) - M_{Jeans}(r_i)\right)^2}{\sigma^2_{M_{HE}}(r_i) + \sigma^2_{M_{Jeans}}(r_i)} \tag{4.1.3}$$

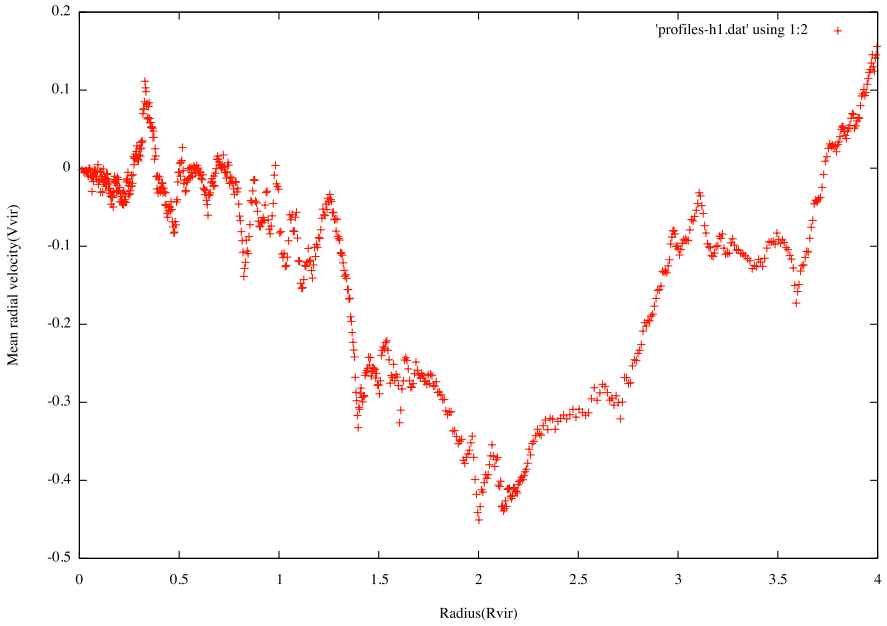

Figure 4.1.1: Mean radial velocity for the DM particles in a cluster given from numerical simulations. This was done for a cluster with $M = 4 \times 10^{14}\mathrm{M}_{\odot}$, $R_{200} = 2\mathrm{Mpc}$ and $v_{vir} = 10^3$ km·s^{-1}. From this numerical simulation, we observe that the radial velocity for the DM particles is almost negligible until we reach the virial radius. This was one of the assumptions that we have made when deriving the Jeans' equation, that the system is motionless on average. In this way we neglected any infall or outflow from DM particles. Note that it is close to the virial radius that the DM particles start to fall towards the cluster. The shift in the velocity at $2R_{vir}$ comes from the expansion of the universe. Credits to Martina Falco.

We test the case which we knew would lead us to $\mathrm{M}_{HE}(r) = \mathrm{M}_{Jeans}(r)$. In our case, this gives us the precision in our numerical simulations: $\chi^2 = 10^{-5}$.

4.1.2 Testing the assumption of hydrostatic equilibrium

Now, we want to study the case when

$$M_{HE}(r) \neq M_{Jeans}(r)$$

Assuming that the condition of hydrostatic equilibrium does not hold, which may be the case for a real cluster, then the hydrostatic mass will be different from the cluster's total mass. In this way, $\mathrm{M}_{Total}(r) = \mathrm{M}_{Jeans}(r)$ and we propose

$$M_{Total}(r) = M_{HE}(r) + \Delta M(r)$$

The concepts that we are about to go through in this short section are not so trivial, and it may confuse the reader. Here, we explain how we simulate $\mathrm{M}_{HE}(r) \neq \mathrm{M}_{Jeans}(r)$. If the reader prefers to skip this intricate discussion, then go directly to

page 36. In page 36, we start explaining the optimisation method which will lead us to $\mathrm{M}_{Jeans}(r) = \mathrm{M}_{HE}(r) + \Delta\mathrm{M}(r)$.

We have derived the "fake" data for the gas, which of course will remain unchanged. Hence, the hydrostatic mass will continue being the same as before, leading us to no other option than to change the Jeans' mass. We continue assuming that $\mathrm{T}_{DM} = \mathrm{T}_g$.

In a first attempt to calculate the Jeans' mass, we will have to calculate the density for the dark matter, assuming that the total mass is given by the hydrostatic mass: $\rho_{DM}(r) = \rho_{HE}(r) - \rho_g(r)$, which in this case gives a NFW model for the dark matter density profile.

Basically, we want to introduce a deviation between the Jeans' and the hydrostatic mass. We do this by choosing a $\beta_{DM}(r)$ that does not translate into the velocity anistropy, chosen to derive the properties of the gas (see app. A.2). We choose $\beta_{DM}(r)$ to be related with $\gamma_{DM}(r) = \frac{\partial \log \rho_{DM}}{\partial \log r}$:

$$\beta_{DM}(r) = -\frac{1}{6}\left(1 + \gamma_{DM}(r)\right)$$

Since $\rho_{DM}(r)$ follows a NFW, β_{DM} continues to be zero in the inner part and changes to 1/3 in the outer part. This difference in $\beta_{DM}(r)$ will induce a difference in $\mathrm{M}_{Jeans}(r)$.

We again compare the agreement between the hydrostatic and the Jeans' mass, and χ^2 goes to 4.67. In fig.4.1.2 we show the hydrostatic and the Jeans' mass. At large radii, the two masses are still the same, and they both give the total mass of the cluster: $M_{Total} = 10^{15} M_{\odot}$. As we move towards the cluster's centre, $\mathrm{M}_{HE}(r)$ becomes different than $\mathrm{M}_{Jeans}(r)$. We want to extrapolate $\Delta\mathrm{M}(r)$:

$$\Delta M(r) + M_{HE}(r) = M_{Total}(r)$$

and

$$M_{Jeans}(r) = M_{Total}(r)$$

The change in the Jeans' mass will be a consequence of relating the dark matter density with the total mass of the cluster. In the case of hydrostatic equilibrium we get the trivial solution of $\Delta\mathrm{M}(r)$ equal to zero, but when we now assume that $\Delta\mathrm{M}(r) \neq 0$, then $\mathrm{M}_{DM}(r) = \mathrm{M}_{HE}(r) + \Delta\mathrm{M}(r)$ - $\mathrm{M}_g(r)$.

Looking at the difference between the hydrostatic mass and the Jeans' mass we start by making an ansatz on the bias in mass $b(r)$ by assuming hydrostatic equilibrium. Recall its definition in eq.(3.1.4), which can be solved in order of the total mass, $\mathrm{M}_{Total}(r) = \mathrm{M}_{HE}(r) + \Delta\ \mathrm{M}(r)$:

$$M_{Total}(r) = \frac{M_{HE}(r)}{b(r) + 1} \tag{4.1.4}$$

where $b(r) \in]-1, 0]$, to prevent $M_{Total}(r)$ to reach unphysical values.

We make an ansatz for the bias, as being a simple function as the one seen in red in fig.4.1.4a, which was somewhat inspired on the bias function obtained in chapter

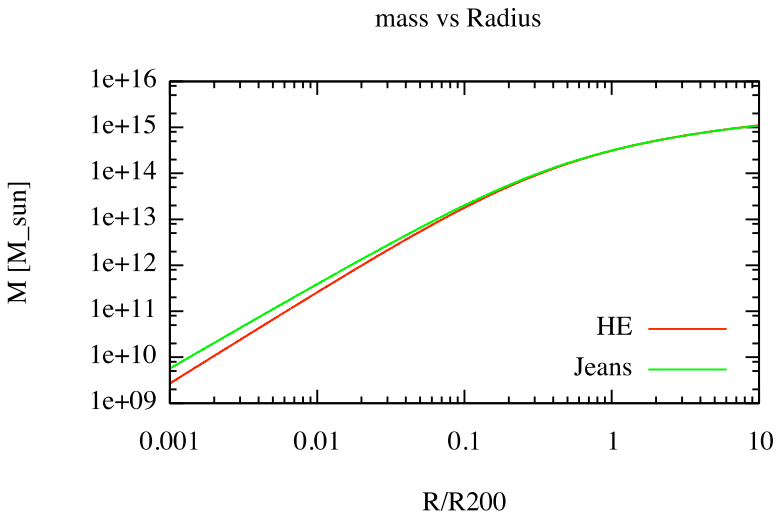

Figure 4.1.2: In red, is the mass calculated under the assumption that the gas is in hydrostatic equilibrium and in green, the mass calculated with the Jeans' equation. The two masses agree at large radii, and because of that we calculate the cluster's total mass under the assumption of hydrostatic equilibrium. The two masses disagree at small radii, we postulate that there must be a ΔM(r) such that, $\mathrm{M}_{HE}(r) + \Delta\mathrm{M}(r) = \mathrm{M}_{Jeans}(r)$.

3.1.2. Making the same calculations as before, we get a $\chi^2 = 100$. From now on, in eq.(4.1.3) one should read M_{Total} where before it was M_{HE}. This tells us that we have made a wrong guess on the ansatz and one that is worse than neglecting the bias. We know that there must be some $\Delta\mathrm{M}(r)$ which translates into having

$$M_{Jeans}(r) = M_{Total}(r) = M_{HE}(r) + \Delta M(r)$$

Since we want to derive a method that leads us to the right $\Delta\mathrm{M}(r)$, we should not expect to make the right guess every time we have access to real data. Therefore, we should develop an optimisation process that can give us the function of the bias, which gives the minimum χ^2.

We could think about taking each data set and randomly assign a value for $\Delta\mathrm{M}(r) \in]-1, max]M_{HE}(r)$ (in principle, we should expect max not to exceed the value 1, so that the bias is not greater than 50% in modulus) and make a random walk at each point. This problem however is not so trivial, given the nature of our calculations, we will have to perform integrations, derivations and fittings, and the neighbouring points are correlated with each other. Trying to find the exact combination for more than 10^3 points (for our simulated data) which minimises χ^2, is simply not feasible.

4.1.3 Optimisation process

The most commonly used optimisation method in Physics to solve such problems, is the Monte Carlo method which takes the advantage of randomness. We choose

a similar approach by implementing the Metropolis Algorithm. With this algorithm, we are capable of exploring the phase-space of configurations without getting trapped into local minima. The advantage of this algorithm is that we assign a probability of accepting a configuration even if it does not follow that χ^2 is smaller than before. A description of the Algorithm, and how it was implemented can be found in app. A.5. In this case we want to look for the bias function that minimises χ^2 so that we get to ΔM: $\mathrm{M}_{Total}(r) = \mathrm{M}_{Jeans}(r) = \mathrm{M}_{HE}(r) + \Delta\mathrm{M}(r)$. In our case, a configuration is defined by a random combination of the free parameters that define the bias function.

From fig. 4.1.2, we see a difference in the Jeans and the hydrostatic mass in the cluster's centre, and not so much in its outskirts. For that reason we will take a simple model for the bias, and set it to zero in the cluster's outskirts, and negative in the center. This is the function that we will adopt to fit and is inspired on the bias function obtained in section 3.2. Such choice of fitting a function with the Metropolis algorithm, instead of a random walk will make the iteration process much faster.

We will take the function of the bias to be constant to a minimum, until it reaches x_0, in the x-axis. From that, it will be increasing linearly until x_1, at the point where it has arrived to a maximum value. We choose b(min) = -99.9% and b(max) = 0. When running the Metropolis Algorithm, we will have x_0 and x_1 as free parameters, and for each iteration there will be a χ^2 associated for a combination of x_0 and x_1, as the one seen in Fig. 4.1.3.

The important thing to collect from this process, is that we calculated ΔM(r) so that end up closer to the equality $\mathrm{M}_{Jeans}(r) = \mathrm{M}_{HE}(r) + \Delta\mathrm{M}(r)$. This was done with the information from the gas temperature and density provided from the simulated data, and with the optimisation process described. In Fig.4.1.4b we show how the total mass $\mathrm{M}_{Total}(r) = \mathrm{M}_{HE}(r) + \Delta\mathrm{M}(r)$ and $\mathrm{M}_{Total}(r) = \mathrm{M'}_{Jeans}(r)$ are again alike. The χ^2-test gives us the value of 0.02, which is a good result.

During the optimisation process we have been relating the dynamical mass with the gravitational mass, as they should be always equal. The final dynamical mass, whether calculated from the dark matter or the gas dynamics, is different from its initial estimation. As a consequence, the gravitational mass will also change. Since we are relying on the X-ray "fake" data to give us the gas mass distribution (which we assume to be spherical), and we consider that the cluster is only built up on gas and dark matter particles then, we will have a different model for the distribution of the dark matter. This is shown in fig. 4.1.5b for the dark matter density, before and after the optimisation. Fig. 4.1.5a represents the mass for the dark matter and the gas.

To calculate ρ_{DM}, we initially took $\mathrm{M}_{Total}(r) = \mathrm{M}_{HE}(r)$ and after optimisation, $\mathrm{M}_{Total}(r) = \mathrm{M}_{HE}(r) + \Delta\mathrm{M}_{optimal}(r)$. We present the fitting parameters to the dark matter density profile under the two different assumptions. A routine was created using gsl functions. Providing the function to be fitted to data, this routine returns the fitting parameters and respective standard deviation, see app. A.4. The results

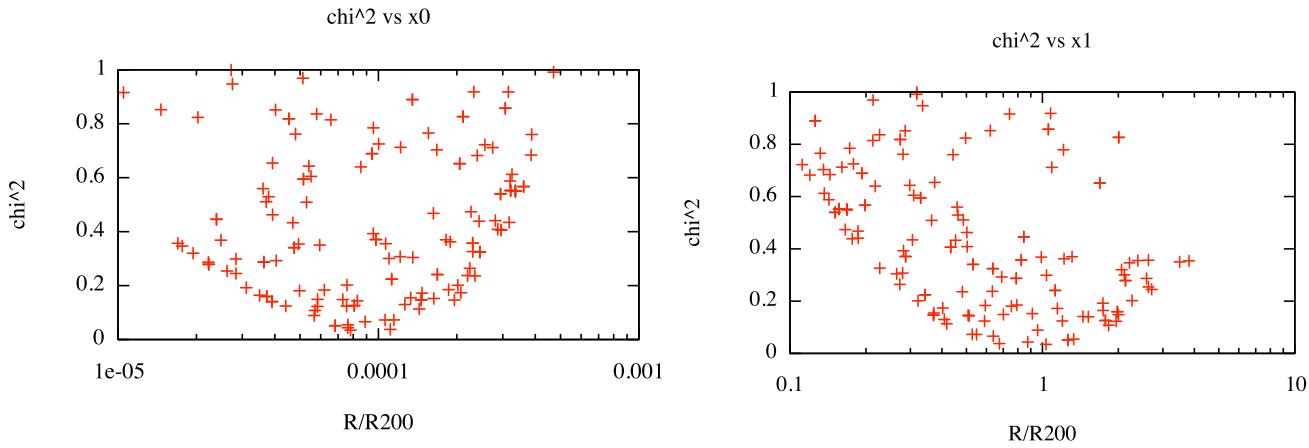

(a) x0 (b) x1

Figure 4.1.3: The best configuration is the one that minimises χ^2. We take the "fake" data for the gas temperature and density and calculate the hydrostatic mass. Expecting the hydrostatic mass to be the total mass, we can then calculate the density for dark matter: $\rho_{DM} = \rho_{HE} - \rho_g$. The Jeans' mass is calculated with ρ_{DM}, $T_{DM} = T_g$ and with β_{DM}. The "fake" data was simulated with $\beta_{DM} = 0$, which gives us $M_{Jeans} = M_{HE}$. By changing β_{DM} to a different profile, $M_{Jeans} = M_{HE} + \Delta M$. We find the ΔM for this specific case by relating ΔM to a bias function, b (in eq. (4.1.4), $\Delta M = M_{Total} - M_{HE}$). We assign two free parameters x_0 and x_1 as described in the text. We show the χ^2-distribution for the different choice of (x_0,x_1). The minimum χ^2 was found to be equal to 0.02 for $(x_0, x_1) = (7.1 \times 10^{-5}, 1.03) R/R_{200}$, in green in fig. 4.1.4a. The χ^2 distribution has the expected shape in lin-log scale as we have taken the random number uniformly distributed in log-scale, see app. A.5, and it is not less than the initial precision in χ^2 (10^{-5}). Moreover, from the law of large numbers, this method will exhibit a $1/\sqrt{n}$ convergence, n being the number of iterations (we chose $n = 500$).

are given along with the error:

parameter	DM initial	DM optimised
ρ_0 (10^{-3} cm^{-3})	10.2 ± 0.6	11.9 ± 0.2
a (Mpc)	0.49 ± 0.03	0.42 ± 0.03
α	0.998 ± 0.003	1.1877 ± 0.0006
β	2.997 ± 0.003	2.927 ± 0.006

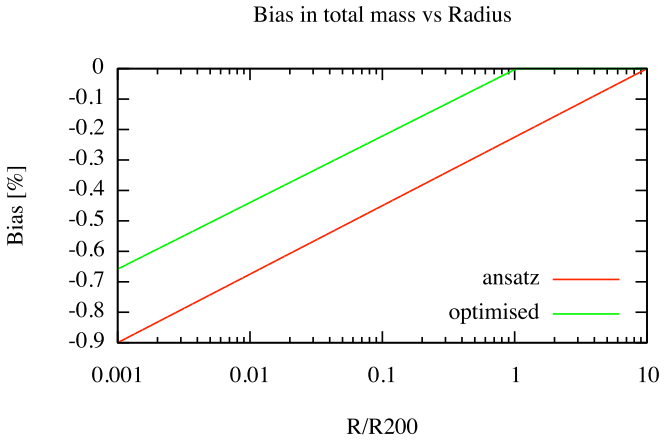

(a) Bias function - before and after

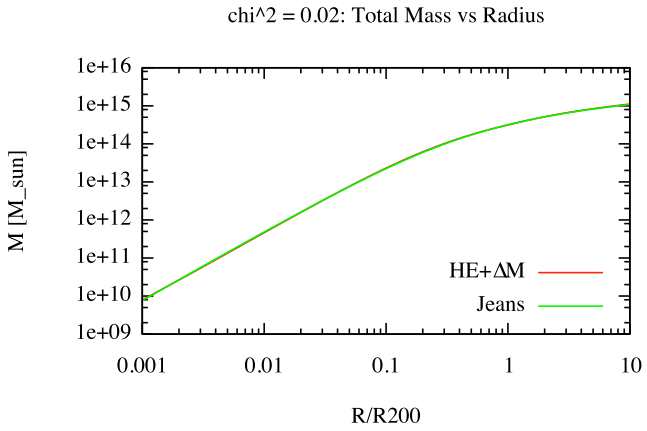

(b) Jeans' and hydrostatic mass - after

Figure 4.1.4: We have estimate a new total mass for the cluster, one that truly describes the total mass of the cluster (when assuming the β_{DM} in question. We have done so by adding $\Delta M(r)$ to $M_{HE(r)}$. $\Delta M(r)$ comes from the optimisation of the bias profile (fig.4.1.4a). This was only possible by relating $M_{Total}(r) = M_{Jeans}(r)$. Furthermore, we have derived the dark matter density profile from $M_{Total}(r) = M_{DM}(r) + M_g(r)$, and assumed that the gas and dark matter "temperature" are the same. Fig. 4.1.4b shows how good do both masses agree, giving a $\chi^2 = 0.02$.

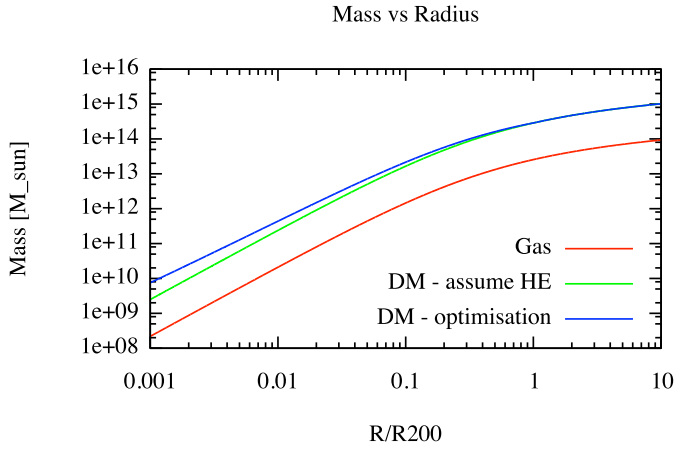

(a) Mass for gas and DM before and after optimisation

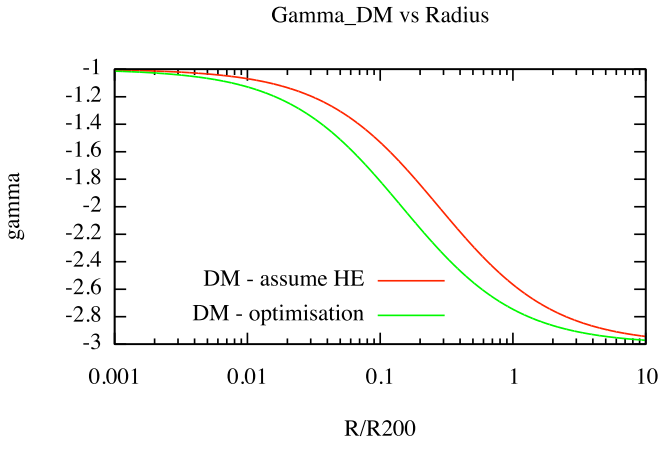

(b) γ_{DM} before and after optimisation

Figure 4.1.5: On the right, fig. 4.1.5b: dark matter density profile ($\gamma = d\log\rho_{DM}/d\log r$) modelled to a double power-law. We see that it follows a NFW. This is the profile as the simulated gas density. We have estimated a new total mass, one that better describes the total mass of the cluster for our choice of β_{DM}. We have done so by adding M_{HE} to ΔM which comes from the optimisation of the bias profile (fig.4.1.4a), by relating M_{HE}, M_{Jeans} and $M_{Total}(r) = M_{DM}(r) + M_g(r)$. In the cluster's outskirts, the relation $M_{DM} = 10M_g$ [35] is still valid, and in the cluster inner part there is more dark matter than previously expected.

4.2 The study of A2052

We will now apply the method derived in the previous section to real X-ray measurements of the A2052. This is an Abell cluster at redshift $z = 0.0348$ [5] with $R_{500} = 1.38 \pm 0.39$ Mpc [24], and the virial radius, $\sim R_{200}$, should be approximately 100kpc further out when in comparison with R_{500}.

Fig. 4.2.1 shows the X-ray image of the region that surrounds A2052. From the X-ray image it is possible to recognise a point source which is associated with the center of the cD galaxy and the central AGN. Having in mind the discussion in chapter 3.1.2, from the presence of the AGN we should expect non-thermal pressure to act back on the gas in the ICM, being this the case we can no longer assume the central region of the cluster to be in hydrostatic equilibrium.

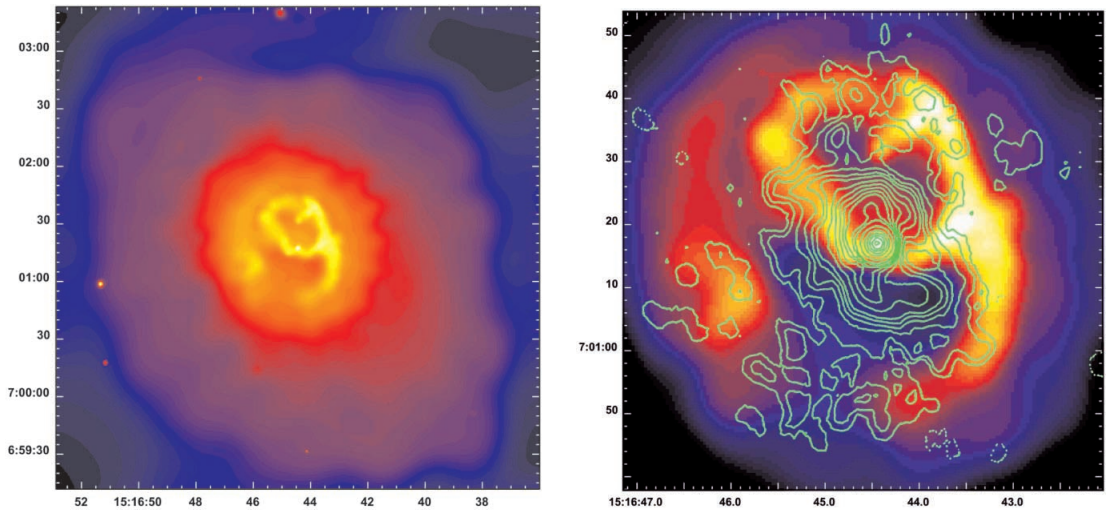

(a) X-rays (b) Radio contours

Figure 4.2.1: Left: Adaptively smoothed image of the region surrounding the center of Abell 2052 from X-ray observations with *Chandra*. Right: Radio contours measured with the *Very Large Array* (VLA). Credits to Blanton et al. [5] and [10].

From the temperature profile (fig.4.2.2), A2052 is defined to be a cool-core (CC) cluster [33]. With the cooling time $t_{cool} \sim 2.6 \times 10^8$yr [5] much shorter than the probable age of the cluster which can give rise to cooling flows. In fig. 4.2.2 we show a possible good fit for the data. For both the gas temperature and density we fit to a double-power law. Note that we have set the outer slope for the temperature $\alpha = 1$. This was a simple way of not allowing the hydrostatic mass to decrease at large radii. For the density profile, we see that we have a good fit, for the temperature profile this could also be the case, if we neglect the last data point.

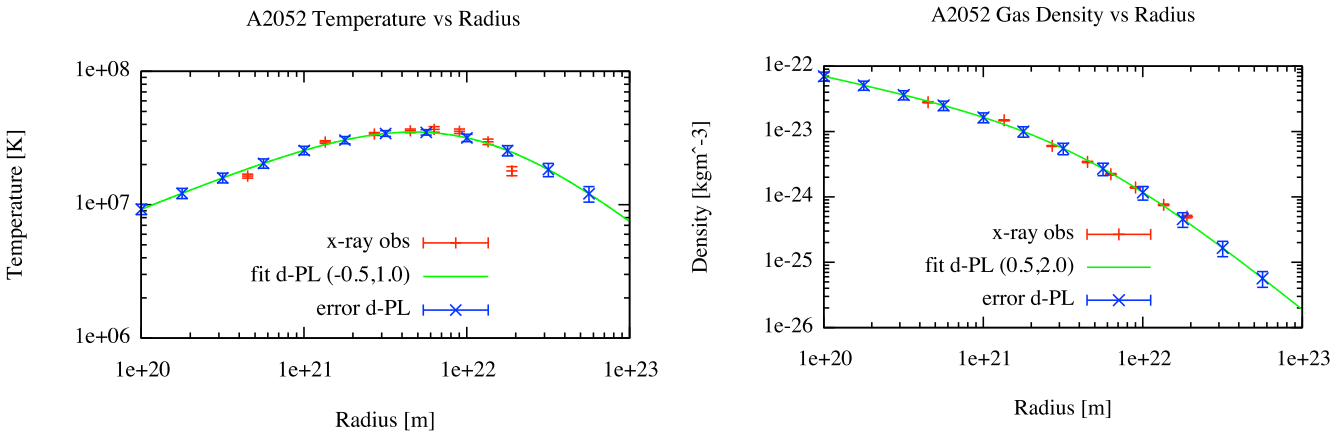

(a) Temperature (b) Density

Figure 4.2.2: We fitted a double power-law (see eq.(1.1.1)) to both the gas temperature and density for the cluster A2052, with fixed parameters (α, β). On the left we fitted (α, β) = (-1/2,1) to $T_0 = (1.8 \pm 0.2) \times 10^8$ K and $r_s = (2.5 \pm 0.4) \times 10^{22}$ m. On the right side of this figure, we have the fit for the density with $(\alpha, \beta) = (\ 1/2,\ 2)$: $\rho_0 = (5.6 \pm 0.7) \times 10^{-24} \mathrm{kgm}^{-3}$ and $r_s = (4.3 \pm 0.5) \times 10^{21}$ m. The error bars in blue were obtained from error propagation from the fitted parameters.

4.2.1 Problem in assuming hydrostatic equilibrium

Assuming the gas in the ICM of A2052 to be spherical[1] and in hydrostatic equilibrium, we can estimate the hydrostatic mass from eq. (2.2.9).

We have taken the set of points for the gas temperature and density and calculated the hydrostatic mass. Unfortunately, there was a problem with this task. The hydrostatic mass decreases when we go to the last data point, and of course, the mass of an object can not decrease as we go further out from its center. This would mean having negative mass, which is physically unacceptable.

The nature of this problem comes from assuming the gas to be in hydrostatic equilibrium at that radius. We should note that the last data point in the temperature drops abruptly, and the hydrostatic mass strongly depends on how the temperature gradient relates to the gradient of the gas' density. We have then taken a different approach, we took a selection of 35 points at each radial bin: both for the temperature and density of the gas. These points were randomly generated from a Gaussian distribution within a 1σ. In this way, 68% of these points are expected to be within the error-bar given from the X-ray measurements, and we could calculate the hydrostatic mass from eq. (4.1.1), fig. 4.2.3 in red.

The cluster's total enclosed mass is $\mathrm{M}(r_{(max)}) = (1.00 \pm 0.13) \times 10^{14} \mathrm{M}_\odot$. Comparing this value with the value in the penultimate point, $\mathrm{M}(r_{(penu,max)}) = (0.93 \pm 0.14) \times 10^{14} \mathrm{M}_\odot$, does not exclude the fact that the hydrostatic mass can decrease when at larger radii. This is another hint that the estimate of the cluster's total

[1]The overall X-ray emission of the thermal gas is fairly circular [5].

mass under the assumption of hydrostatic equilibrium may not be the right one.

4.2.2 Comparing collisional with collisionless (one last time)

We have previously compared the cluster's dynamics for a collisional (gas) and collisionless (DM) systems. We have seen that if the assumption on the derivation of the Jeans' and the hydrostatic equilibrium equation are true for the cluster in question, then $M_{HE}(r) = M_{Jeans} = M_{Total}(r)$ should hold.

To derive the Jeans' mass, we begin by estimating the dark matter density profile: $\rho_{DM}(r) = \rho_{Total}(r) - \rho_g(r)$, see fig.4.2.8 (blue), where we have taken the total density from $M_{Total}(r) = M_{HE}(r)$. We are still left with two unknown parameters which are not possible to measure. We make the key assumption that $T_{DM}(r) = T_g(r)$:

$$\sigma_r^2(r) = \left[\frac{\mu m_p}{k_B}\left(1 - \frac{2}{3}\beta_{DM}(r)\right)\right]^{-1} T_g(r)$$

For the β_{DM} profile, we have carried out two different studies, one with $\beta_{DM}(r) = 0$, and another with $\beta_{DM}(r) = 1/3$, inspired on the work of Hansen & Piffaretti [20] for the case study of A2052. With this we calculate the Jeans' mass using the Jeans' equation (2.1.14), and we can then compare this mass with the hydrostatic mass (see fig. 4.2.3).

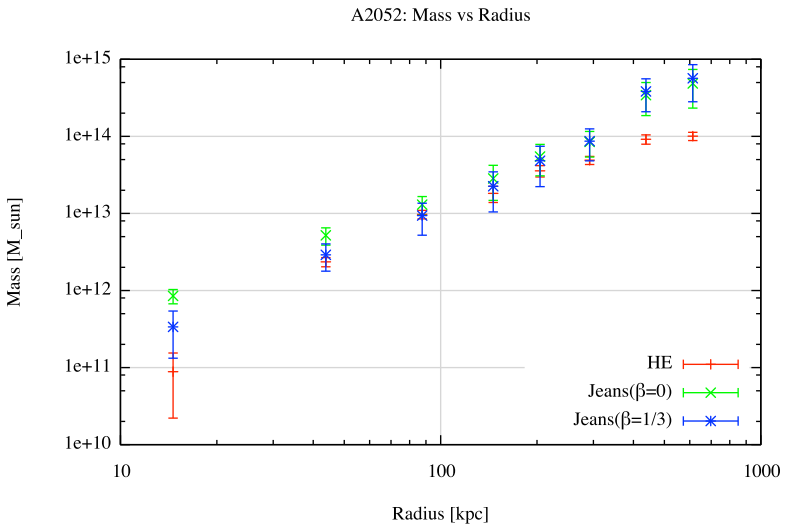

Figure 4.2.3: We give the hydrostatic mass and respective error. Assuming that this mass is the cluster's total mass, then we obtain the dark matter density profile which can be seen in comparison with the gas: $\rho_{DM} = \rho_{Total} - \rho_g$, fig. 4.2.8. We also plot the Jeans' mass, taken from the dark matter density profile and assuming, $T_{DM} = T_g$. We show two different results for two different assumptions on β_{DM}: $\beta_{DM} = 0$ and $\beta_{DM} = 1/3$.

In fig. 4.2.3 we see that they do not agree at the cluster's inner and outer radii. Close to the virial radius, which is where we estimate the total mass of the cluster,

the hydrostatic and the Jeans' mass do not agree. Therefore, we no longer expect that with the hydrostatic equilibrium equation (4.1.1), we get the total mass of the cluster.

In chapter 3.1.2, we showed that the gas motion and non-thermal pressure can be relevant for the cluster dynamics. From the X-ray image we do not expect the cluster to be in hydrostatic equilibrium in its centre (strong radio source) and in its outskirts (infalling accreting gas). We accounted for this effect as a ΔM: $\mathrm{M}_{Total}(r) = \mathrm{M}_{HE}(r) + \Delta\mathrm{M}(r)$. In eq.(3.3.4) we have written the full expression of ΔM.

In fig. 3.3.1, we showed that the effect of non-thermal pressure and the gas' velocity may be non-negligible in the inner and outer radii, which is what we are now observing when comparing the Jeans' with the hydrostatic mass, see fig. 4.2.3. Note that, if we want to make any comparison between both figures, we should constrain it to the radius where we can have trustful X-ray measurements, typically from $[0.01,1]\mathrm{R}_{200}$. We had our definition of the bias in the cluster's true mass when assuming hydrostatic equilibrium:

$$b(r)_{[\%]} = -\frac{\Delta M(r)}{M_{Total}(r)} \times 100 \tag{4.2.1}$$

Nevertheless, from X-ray observations, we know nothing about the origin neither can we directly measure the contribution of ΔM to the cluster's dynamical mass.

4.2.3 The degeneracy in β_{DM}

Let us first look at the difference in the Jeans' mass for the two different β_{DM} models and see if it can explain ΔM.

When we make a χ^2-test[2] we have a clear difference in the different choice of β_{DM}: $\chi^2 = 24.9$ for $\beta = 0$ and $\chi^2 = 7.75$ for $\beta = 1/3$. In section 4.1, we have seen that the change in this parameter could be responsible for the difference in both masses.

The difference in the Jeans' mass from choosing $\beta_{DM} = 1/3$ and 0, seems to be only relevant at the inner radii. When $\beta_{DM} = 1/3$ we have that the Jeans' mass is closer to the hydrostatic mass at inner radii, than when setting it to be zero. When we change $\beta_{DM}(r)$, it means that in the Jeans' equation (4.1.2) we change

$$\frac{d\log\rho_{DM}}{d\log r} + \frac{d\log\sigma^2_{DM}}{d\log r} + 2\beta_{DM}(r) = \gamma_g(r) + \gamma_{\sigma^2_r}(r) + 2\beta_{DM}(r) \tag{4.2.2}$$

Assuming that we have a NFW model (1.1.1) for the dark matter density profile, its contribution to the equation above mentioned will be -1 in the inner part ($R < r_s$) and -3 for the outer part ($R > r_s$). In app. A.1 we show $\gamma_{T_g} = \gamma_{\sigma^2_r}$, see fig.

[2]We are no longer using the reduced χ^2-test. For this reason we do not divide by N (the number of radial bins) in eq. (4.1.3)

A.2.1, which comes from assuming that the gas and dark matter temperature are the same. From the fit to the temperature of the gas, fig. 4.2.2a, we should then have $\gamma_{\sigma_r^2} \sim 1/2$ for inner part and $\gamma_{\sigma_r^2} \sim -1$ for the outer part of the cluster. When we add γ_g and $\gamma_{\sigma_r^2}$, we have the solution of $\sim -1/2$ and ~ -4 for the inner and outer part, respectively. From numerical simulations of galaxy clusters, we expect $-1/2 \leq \beta_{DM}(r) \leq 1/2$. We then see that, in the Jeans' equation, the choice of β_{DM} is relevant at small radii, and at larger radius $\gamma_g + \gamma_{\sigma_r^2}$ dominates over β_{DM}, making this choice less relevant.

We could then argue that this profile bring us closer to the one needed to describe the dark matter and that at the same time it allows the gas in the ICM to be in hydrostatic equilibrium. We try to tune $\beta_{DM}(r)$ towards $M_{HE}(r) = M_{Jeans}(r)$, for the observed region in the cluster.

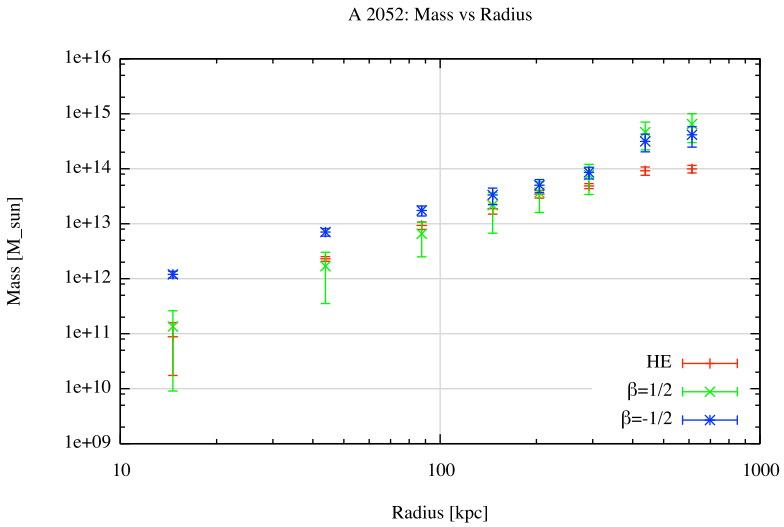

Figure 4.2.4: Difference in the inner part

In fig. 4.2.4 we show the comparison between the hydrostatic mass and the Jeans' mass, assuming $\beta_{DM} = 1/2$ and $\beta_{DM} = -1/2$. For $\beta_{DM} = 1/2$ the Jeans' and the hydrostatic mass agree at small radii, and not much was improved at larger radii. Setting $\beta_{DM} = -1/2$ makes a slight difference at larger radii, which we have above discussed. Just by looking at the error-bars, we see that the χ^2 decreases for the first choice of β_{DM}. We conclude that the choice of β_{DM} will indeed have an impact on the result given by the Jeans' equation (2.1.14) and a wrong choice of β_{DM} could be the reason behind the difference observed between the Jeans' and the hydrostatic mass.

Nevertheless, we should also consider that the difference between the Jeans' and the hydrostatic mass could also come from the effect of non-thermal pressure and the gas motion on the dynamical mass as we showed in chapter 3.1.2. For this reason, it is important to note that not only have we observed a degeneracy in the influence of magnetic fields and cosmic rays at small radii, but now we also have a

degeneracy in the choice of β_{DM}.

The degeneracy is lifted in the outermost part of the cluster, see the discussion in eq. (4.2.2). We see that the choice of β_{DM} does not affect the Jeans' mass much at large radii, for the choice of $-1/2 < \beta_{DM} < 1/2$. The major contribution to the difference between both masses comes from the non-thermal pressure. From what we have studied, we know that at larger radii, the effect of the velocity of the gas gives a larger contribution to the dynamical mass than the pressure support from magnetic fields and cosmic rays. For this reason, if we can calculate ΔM close to the virial radius, than not only do we get a better estimation for the total mass of the cluster but also, we can have an estimation of the velocity of the gas at that radius.

4.2.4 "Extra" dynamical mass

In section 4.1.3, we derived a method capable of extracting ΔM from X-ray measurements alone (the "extra" dynamical mass which is not accounted for in the Hydrostatic equilibrium (HE) eq.). This method was derived taking the gas' temperature and density profile, and ΔM optimised, so that we end up with $\mathrm{M}_{HE} + \Delta\mathrm{M} = \mathrm{M}_{Jeans} = \mathrm{M}_{Total}$ [3]. The method derived will now be used for the particular study of A2052.

To use the routine built in the previous section, we need first to make a choice on the shape of the bias, $b(r)$. In section 3.1.2 we studied the overall contribution that we can have from non-thermal pressure and the gas' motion could have to the cluster's mass. In particular, fig. 3.3.1 shows the bias in mass when assuming hydrostatic equilibrium. From the choice in the models, the bias function had a shape that can be simplified to a hat-function, linearly increasing and then decreasing function ($x_0 < x_1 < x_2 < x_3$, m_x and b_x are fitted to make it as a continuous function):

$$b(r) = \begin{cases} min & \text{if } r < x_0 \text{ and } r > x_3 \\ m_0 r + b_0 & \text{if } x_0 > r > x_1 \\ max & \text{if } x_1 > r > x_2 \\ m_1 r + b_1 & \text{otherwise} \end{cases}$$

We now assume, that this function for the bias is the one that we may have for the cluster A2052, this can in principle be true. We generalise this problem by dividing the hat-function into two functions: $\mathrm{b(r)} = b_{left}(\mathrm{r}) + b_{right}(\mathrm{r})$,

$$b_{left}(r) = \begin{cases} min & \text{if } r < x_0 \\ max & \text{if } r > x_1 \\ m_0 r + b_0 & \text{otherwise} \end{cases}$$

[3] Being an optimisation process, we actually get $(\mathrm{M}_{HE} + \Delta\mathrm{M}) \sim \mathrm{M}_{Jeans}$ and not the equality.

$$b_{right}(r) = \begin{cases} min & \text{if } r < x_2 \\ max & \text{if } r > x_3 \\ m_1 r + b_1 & \text{otherwise} \end{cases}$$

Both b_{left}(r) and b_{right}(r) are similar to the bias function that was used in section 4.1.3. For this reason, we take the same code, adjusting it slightly. First, the code will have to be run twice, one for b_{left} and another for b_{right}. For each we run, we are fitting the combination (x_i, x_j) that minimises χ^2. Note that we allow $x_1 > x_2$.

To fit the free parameters (x_0, x_1, x_2, x_3), we take the minimum and maximum plateau to be -99.9% and 99.9% respectively. We take the first five and the last five set of data for A2052 and optimise $b_{left}(r)$ and $b_{right}(r)$, respectively. For each run of the Metropolis we will have b(r) = b_{left}(r) + b_{right}(r). Note that, overall we were given eight set of data, meaning that the left- and right-functions have two common points. We do this so that we can have a correlation between these two functions, when summing them together.

In fig. 4.2.5, we show the result obtained from running the algorithm at each resolution for the random Gaussian distribution. We have also try to optimise different combinations of $b_{right}(r)$ and $b_{left}(r)$, but our first choice seems to give the minimum χ^2, for the particular case of this cluster. Remember, that we define χ^2 as a measure for the difference between M_{Jeans} and $M_{HE} + \Delta M$ (eq.(4.1.3)), where Δ M changes according to the choice of $b(r)$, see eq. (4.1.4).

To account for the systematic error that we have from the different choice of β_{DM} and for the statistical error that comes from the Gaussian distribution of data within the 1σ. We estimate the error in the bias: $\sigma^2 = \sigma^2_{stat} + \sigma^2_{syst}$. In fig. 4.2.6 we account for this error and show a better plot of the bias in the hydrostatic mass along the cluster.

From the bias, we can make an estimation about the cluster's true mass. Fig. 4.2.7a and fig. 4.2.7b, show that the Jeans' mass and the new dynamical mass (M_{HE}+ΔM), can be similar to each other which give us a better estimation of the cluster's total mass, than simply assuming the gas in the ICM to be in hydrostatic equilibrium. And this method can now be applied to other clusters.

From the bias at the virial radius: $b(r_{max})$=-0.48 ± 0.13 and $M_{HE}(r_{max}) = (9.98 \pm 1.4) \times 10^{13} M_\odot$, we calculate ΔM given by eq.(4.1.4): $\Delta M = (r_{max}) = (9.2 \pm 3.8) \times 10^{13} M_\odot$.

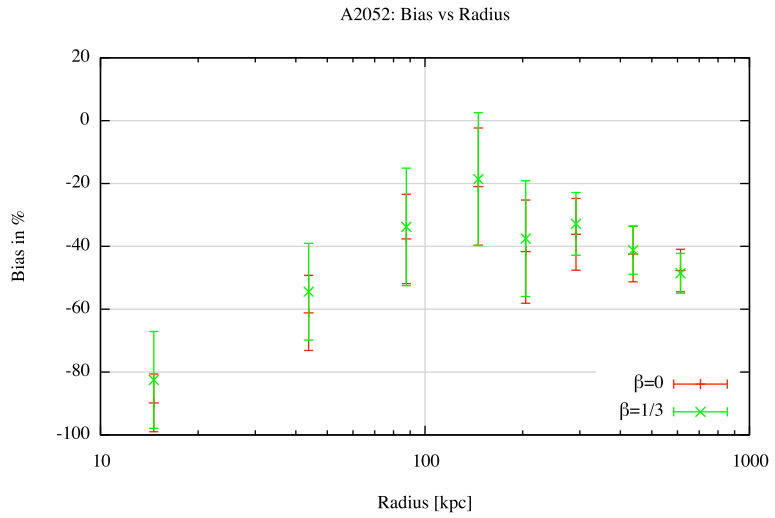

Figure 4.2.5: Bias in the true mass of the cluster when neglecting ΔM. In the inner part, the bias can be of the order of -70% to -100% depending on the choice of β_{DM}. This bias, not only comes from the choice of β_{DM} but also due to the presence of magnetic fields or cosmic rays and some infall of the gas towards the cluster's centre. Close to the scale radius, this bias is less relevant. This tell us that the influence of non-thermal pressure to the cluster's dynamical mass is no longer relevant beyond this radius. The bias at the outermost radii is dominated from the effect of the gas' velocity in the ICM. Therefore, from the bias, we can infer about the order of magnitude of the velocity of the gas at such radius.

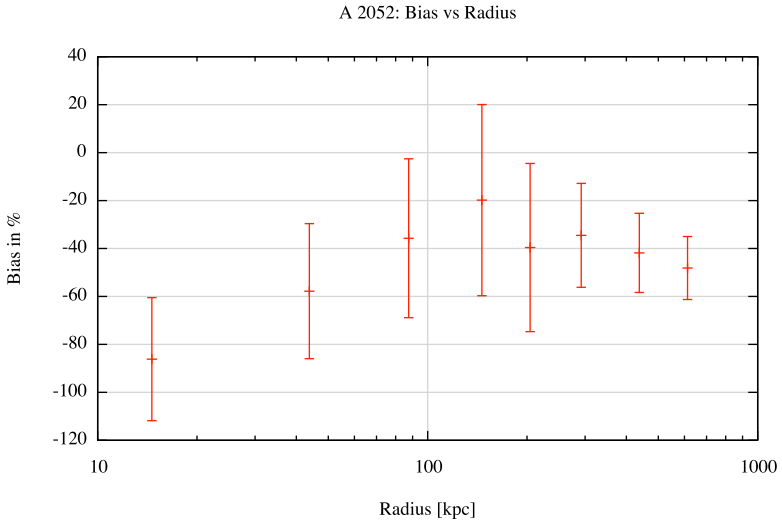

Figure 4.2.6: Bias in Total mass when assuming hydrostatic equilibrium. The error bars now account for the systematic error on the different choice of β_{DM}: $\sigma = \sqrt{\sigma^2_{stat} + \sigma^2_{syst}}$. At each point we took $\sigma^2_{stat} = max(\sigma^2_{\beta=0}, \sigma^2_{\beta=1/3})$.

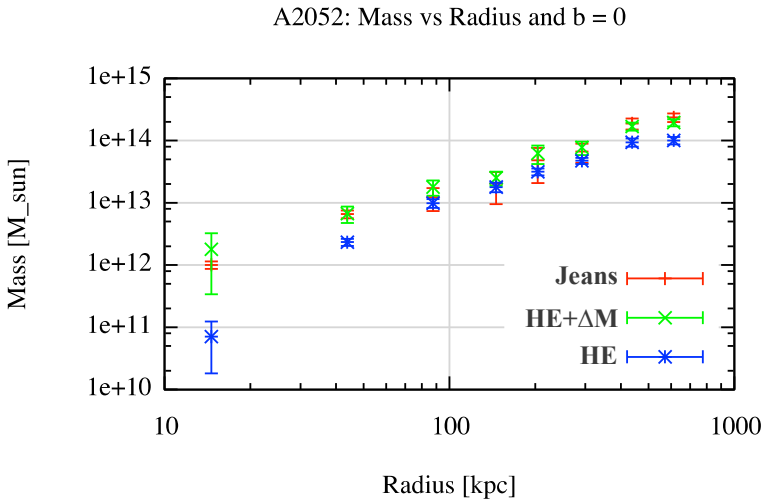

(a) M_{Jeans} & M_{HE}+ΔM when $\beta_{DM} = 0$

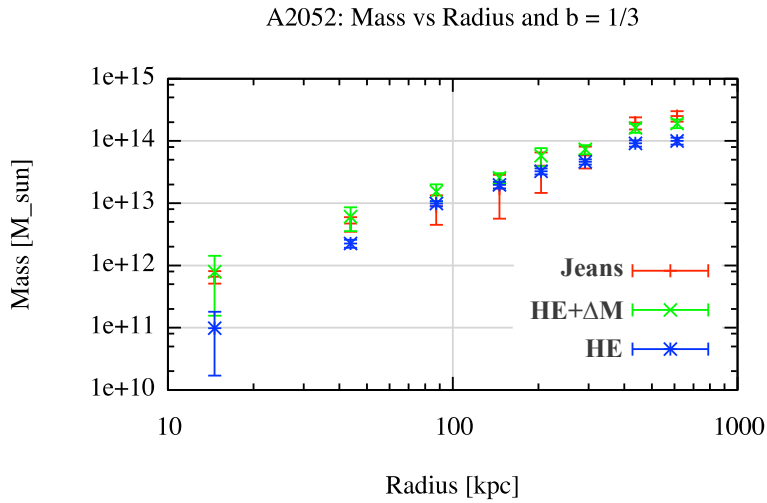

(b) M_{Jeans} & M_{HE}+ΔM when $\beta_{DM} = 1/3$

Figure 4.2.7: Comparison between M_{Jeans} and M_{HE}+ΔM, for the two different cases of choosing $\beta_{DM} = 0$ and $\beta_{DM} = 1/3$. We see that we finally have $M_{Jeans} = M_{HE}$+ΔM. In this way, we have derived a method that can give us a better estimation about the cluster's total mass from X-ray observations only, than considering the gas to be in hydrostatic equilibrium. For comparison, we also show the hydrostatic mass.

4.2.5 The Dark Matter halo

We have been arguing that if we assume the gas in the ICM to be in hydrostatic equilibrium, then there is a mass, ΔM, that is not been taken into account, as a consequence of considering the full dynamics of the cluster. Moreover, we must have a one to one correspondence between the cluster's dynamical mass and the cluster's gravitational mass. Hence, if we now have an extra-ΔM in the dynamical mass, this factor should also be added to the gravitational mass.

Since the gas' mass is estimated from X-ray measurements of the gas' density assuming spherical symmetry, it remains invariant under any of our assumptions. From simple calculus, we then conclude that we what we are changing is our perception on how is the dark matter distributed along the cluster. For A2052, we have more dark matter in the ICM, than previously assumed with hydrostatic equilibrium of the gas: $\mathrm{M}_{DM}(r) = \mathrm{M}_{Total}(r) - \mathrm{M}_g(r)$. At the cluster's centre this may be overestimated. We know that A2052 hosts a cD galaxy at its centre[4], and we see in fig.4.2.8, that there is not a smooth transition in the dark matter density from the first to the second data point. At the cluster's outer part there is only gas and dark matter, and with our method there is a new distribution of the dark matter halo.

Fig.4.2.8, shows the dark matter density profile and how it changes under the three different assumptions, after the optimisation process: $\mathrm{M}_{Total}(r)=\mathrm{M}_{HE}(r)$ (blue), $\mathrm{M}_{Total}(r)=\mathrm{M}_{HE}(r)+\Delta\mathrm{M}_{\beta=1/3}(r)$ (green) and $\mathrm{M}_{Total}(r)=\mathrm{M}_{HE}(r)+\Delta\mathrm{M}_{\beta=0}(r)$ (red). To recover the density profile from the mass, we assume spherical symmetry, eq. (A.1.7).

4.2.6 Constraint on the cluster's dynamics

The work develop during this thesis project has come to terms to its main goal: to better constraint the dynamics of a cluster. Making it possible to better estimate the total mass of a cluster, which is not in hydrostatic equilibrium close to the virial radius. Furthermore, this can also give us some insight of the motion of the gas in the ICM.

Total Mass

We have derived a method that accounts for any deviation in the total mass, when compared to the hydrostatic mass calculated with X-rays measurements alone.

The cluster's dynamical mass, can be estimated with the derived method:

$$M_{Total}(r) = M_{HE}(r) + \Delta M(r)$$

ΔM(r) is the missing mass that is extracted with the method derived (generalising, ΔM(r) could also give a "negative mass").

[4] $\mathrm{M}_{DM}(r) = \mathrm{M}_{Total}(r) - \mathrm{M}_g(r)$ - M_{stars}.

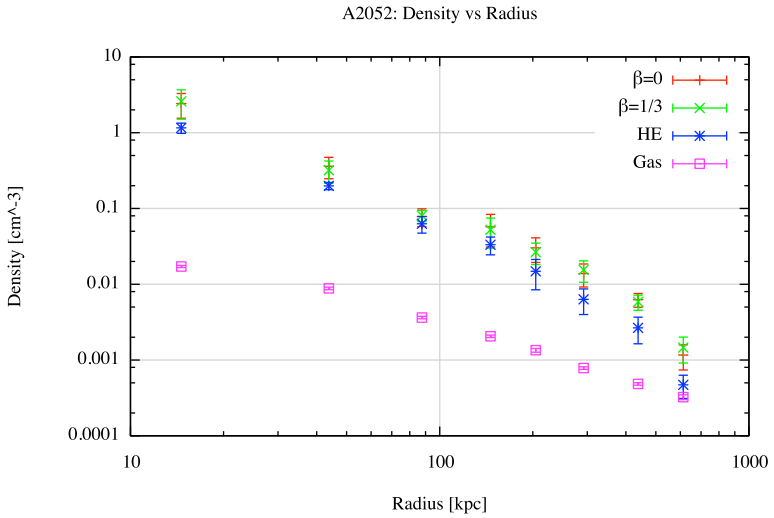

Figure 4.2.8: Density of the gas obtained from X-ray measurements. Comparison with the density of dark matter, under the assumption of hydrostatic equilibrium and after the optimisation process for the two different choices of β_{DM}. We have constrained the total mass to always be bigger than the gas' mass to prevent any non-physical result. The dark matter density profile can be fit to a NFW. In the cluster's outskirts the relation $M_{DM} \sim 10\ M_g$ [35], assume spherical distribution of matter. In the inner part we have a denser region of dark matter than expected when assuming hydrostatic equilibrium.

For the study of A2052, we calculate

$$M_{HE}(r_{max}) = (0.99 \pm 0.14) \times 10^{14} M_{\odot}$$

and estimate $\Delta M(r)$, considering statistical and systematic errors:

$$\Delta M(r_{max}) = (0.92 \pm 0.38) \times 10^{14} M_{\odot}$$

The estimate for the total mass of A2052 with this novel method, gives

$$M_{Total} = (1.92 \pm 0.40) \times 10^{14} M_{\odot}$$

This is an impressive result. We show that for the particular study of A2052, the total mass is twice the hydrostatic mass which is quite a significant difference. This result lead us to conclude that for clusters, which have not yet reached hydrostatic equilibrium at the virial radius, current measurements of the hydrostatic mass can not be compared to the cluster's mass, otherwise we would be working with the wrong physics. We strongly advise applying this methods to X-ray measurements of other clusters, and measure the cluster's total mass again, only now, do this by applying the method shown in this thesis.

Gas motion

We have been studying the dynamics of a galaxy cluster, and what could possibly be powering the cluster, to not let it settle to a state of hydrostatic equilibrium. We

found that non-thermal pressure and the velocity of the gas are responsible for this. We can now try to measure their contribution to the cluster's dynamical mass, by measuring the difference between the cluster's dynamical mass and its hydrostatic mass, which we defined as a $\Delta M(r)$.

In chapter 3.1.2, we showed that, by only looking $\Delta M(r)$, it is not possible to distinguish between the magnetic field and cosmic rays pressure as their signature in $\Delta M(r)$ are the same. Moreover, we assume that their contribution is mostly relevant in the cluster's inner part, where the degeneracy with β_{DM} can not be neglected.

With the result obtained for the bias function, fig. 4.2.6, we see that the A2052 reaches hydrostatic equilibrium (where the bias is close to zero) at $R \sim 100$kpc, and when we look further at $R \sim 200$kpc, this is no longer the case. Based on the bias function extracted from our method, this is how we picture the dynamics of this cluster to be:

- At the cluster's centre we have the presence of magnetic fields, cosmic rays and the gas is not static. So close to the centre, the bias represents an underestimation of the hydrostatic mass of 60% up to 100% [5]. We can not make constraints on the intensity of the magnetic field, the abundance of cosmic rays or even the turbulent motion due to the degeneracy between them, and β_{DM}. Besides, we would have to trouble ourselves to solve eq. (3.2.5) to recast them from $\Delta M(r)$, which concerning all the three factors in this equation, it is impossible to solve it without other measurable quantities with other observational methods.

- As the bias function starts to increase (from negative values to zero), the non-thermal pressure decreases, and the gas particles start to become motionless on average. This is most likely to be the case, as the non-thermal contribution for the bias is always negative. Doubtfully, would we expect that the gas to suddenly change its motion to balance the bias from non-thermal pressure. We reach hydrostatic equilibrium when $b(r) \sim 0$.

- When $R \gtrsim 200$kpc, ΔM starts to increase again, showing that the gas is driven away from hydrostatic equilibrium. Rudnick et al. discuss on a recent paper, that the radio halos measured outside the cluster core (rotation measurement (RM), see app. B.3), could come from shocks of the plasma and its turbulent character along the connecting filaments, and not from the magnetic field strength. For this, we will only consider the velocity of the gas, at such radius.

We are now able to constraint the velocity of the gas at the cluster's outskirts from the estimated ΔM. The relation between the gas' velocity and ΔM is given by eq. (3.1.2):

$$\Delta M = \frac{r}{G}\left(v_\theta^2 + v_\phi^2 - r v_r \frac{dv_r}{dr}\right)$$

[5] We are not considering the non-physical result of $b(r)_{[\%]} < -100\%$.

It becomes possible to get an estimation of the bulk rotation and motion of the gas at this radius:

$$\frac{\Delta M}{M_{Total}} \sim \frac{v_\theta^2 + v_\phi^2 - v_r \frac{dv_r}{dr}}{\sigma_r^2} \Rightarrow \tag{4.2.3}$$

$$v_\theta^2 + v_\phi^2 - v_r \frac{dv_r}{dr} \sim \sigma_r^2 \frac{\Delta M}{M_{Total}} = -b\sigma_r^2 \tag{4.2.4}$$

From the gas' temperature we infer about the velocity dispersion for dark matter, eq. (A.1.13):

$$\sigma_r^2 = \left[\frac{\mu m_p}{k_B}\left(1 - \frac{2}{3}\beta_{DM}\right)\right]^{-1} T_g$$

Substituting this in eq. (4.2.4), we get:

$$|v_\theta^2 + v_\phi^2 - v_r \frac{dv_r}{dr}| = (3.0 \pm 0.8) \times 10^2 km \cdot s^{-1} \tag{4.2.5}$$

We have set a constraint to the bulk motion and rotation of the gas close to the virial radius. Until today, if we wanted to measure the velocity of the gas at this radius with such accuracy, this could only be done from high-resolution numerical simulations as done by Norman and Bryan [30] which result gives $v_{turb} = 300 - 600 \mathrm{km \cdot s^{-1}}$, which are in good agreement with the result obtained with this method.

Chapter 5

Discussion

Galaxy clusters at the virial radius, may not obey the condition of hydrostatic equilibrium. This assumption, is commonly used when we want to measure the mass of clusters with X-ray observations.

Cluster which are still undergoing mergers, suffer from the motion of the infalling gas or outflow and this will contribute dynamically to the cluster's total mass. Moreover, it can also happen that the magnetic and cosmic ray pressure acting on the plasma approaches the thermal pressure. Consequently, it is not possible to retrieve information about the gravitational mass of the cluster, assuming that the gas in the ICM is in hydrostatic equilibrium.

In section 4.1, we show that it is possible to recover the dynamical mass from X-ray measurements. We take the X-ray measurements and relate the dynamics of the gas with the dark matter. We assume that the gas and dark matter are spherical, and that the dark matter is in static equilibrium. This method relies on the key assumption that we can relate the temperature of the gas with the dark matter. In particular, we take $T_{DM}(r) = \kappa(r)T_g(r)$ with κ always equal to one. Numerical simulations show that κ varies less than 20% with radius: $\kappa(r) \in [0.9,1.2]$ [23, fig. 1]. This change in $\kappa(r)$ is not so straightforward to implement, but is fundamental in our method. For now, we take the consequences of our choice and leave it as an open problem.

In summary, with this novel method, we no longer need to assume the cluster to be in hydrostatic equilibrium to get an estimate of the cluster's total mass if we want to rely on X-ray measurements alone. We apply this method to A2052 and find that the total mass of the cluster is almost twice the hydrostatic mass at the virial radius. This difference is extremely significant, and we can not be neglected if we want to better constrain the cosmological parameters. By applying this method, we can potentially measure Ω_m more accurately. Hence, giving us more information about the content of dark matter and dark energy in the universe.

Furthermore, there have been attempts to calculate the velocity of the gas, magnetic fields and cosmic rays in galaxy clusters. With this method, we can constrain their contribution to the cluster's dynamics. Close to the virial radius, the velocity

of the gas is responsible for the observed difference in the cluster's total mass, and with this difference, we were able to constrain the velocity of the gas close to the virial radius, for A2052. It is the first time, this is done so straightforward, and with such precision.

Appendix Overview

The structure of this appendix is as follows:

Appendix A - we go through some of the most important calculations to built the functions necessary in our coding, and also how to simulate the "fake" data for the gas density and temperature for a galaxy cluster. It ends by describing the libraries and routines, that were written for this work. Apart from "gsl", everything was written from the very beginning. using C programming.

Appendix B - this appendix is related to observations of galaxy clusters. We briefly mention X-ray observations, since this was already so discussed during the course of this thesis. We continue by describing the physics behind radio observations, and how it can be related to cosmic rays and magnetic fields in the ICM. Finally, we end by mentioning how others have been trying to measure the velocity of the gas in clusters.

Appendix C - a description of vector calculus in spherical coordinates and a short explanation about the divergence theorem.

Appendix A

Galaxy Cluster Dynamics

A.1 Calculus for Galaxy clusters

Mass assuming spherical symmetry The mass of a homogeneous object can be determined in terms of its density, in spherical coordinates :

$$M_j(r_i) = \int \rho_j(r')dr'd\Omega = 4\pi \int_0^{r_i} \rho_j(r')r'^2 dr' \tag{A.1.1}$$

When referring to a certain quantity X assigned to j we use the notation X_j, where j can be *g, DM* or t is the short notation for gas, dark matter and total contribution of species in the galaxy cluster, respectively.

Density from cluster's total mass

We see that if we know the total mass and the temperature for the gas, it becomes possible to derive the density for the gas, all we have to do is to invert Eq. (2.2.9) and take the integral over the limits. The same is true for the dark matter if we invert Eq. (2.1.14) and instead of the temperature we are given a dispersion velocity and β_{DM} profile:

$$\gamma_g(r) = \frac{d\log\rho_g}{d\log r} = -\frac{d\log T}{d\log r} - \frac{G\mu m_p}{k_B}\frac{M_t(r)}{rT(r)} \tag{A.1.2}$$

$$\gamma_{DM}(r) = \frac{d\log\rho_{DM}}{d\log r} = -\frac{d\log\sigma_r^2}{d\log r} - 2\beta(r)\frac{GM_t(r)}{r\sigma_r^2(r)} \tag{A.1.3}$$

$$\rho_j'(r_i) = \rho_j'(r_0)\exp\left(\int_{r_0}^{r_i}\gamma_j(r)d\log r\right) \tag{A.1.4}$$

Where we assign $\rho_j'(r_0)$ to be equal to a random number. We normalise the density since we know from observations that typically the gas mass fraction (M_g/M_{HE}) gives $M_g(r_{max}) = 0.1M_{DM}(r_{max})$, [35] hence we normalise the gas density:

$$M_g(r_i) = \frac{1}{10}\frac{M_{DM}(r_{max})}{M_g(r_{max})}M'_g(r_i) \tag{A.1.5}$$

Under the same principle, the following condition should be verified when we generate a pseudo dark matter mass ($M'_{DM}(r)$):

$$M_{DM}(r_i) = 10\frac{M_g(r_{max})}{M_{DM}(r_{max})}M'_{DM}(r_i) \tag{A.1.6}$$

A density profile can then be obtained from the normalised mass by taking the derivative of Eq. (A.1.1).

$$\rho_j(r_i) = \frac{1}{4\pi r_i^2}\frac{dM_j}{dr} \tag{A.1.7}$$

Velocity Dispersion for dark matter

Velocity dispersion for dark matter can be obtained from Jeans equation (2.1.14) in spherical coordinates:

$$\sigma_r^2(r_i) = \frac{G}{\tilde{\rho}(r_i)}\int_{r_i}^{\infty}\frac{\tilde{\rho}(r')M_t(r')}{r'^2}dr' \tag{A.1.8}$$

With the introduction of a new parameter $\tilde{\rho}$ and taking $\rho(r_{min})/\tilde{\rho}(r_{min}) = 1$

$$\frac{d\log\tilde{\rho}}{d\log r} = \frac{d\log\rho}{d\log r} + \frac{2\beta(r)}{d\log r}d\log r \Rightarrow \tilde{\rho}(r) = \rho(r)\exp\left(\int_{r_{min}}^{r} 2\beta(r')d\log r'\right) \tag{A.1.9}$$

We can re-write Jeans equation (2.1.14) as

$$M(<r) = -\frac{r\sigma_r^2(r)}{G}\left(\frac{d\log\left(\tilde{\rho}\sigma_r^2\right)}{d\log r}\right) \tag{A.1.10}$$

and solve Eq. (A.1.10) with respect to the velocity dispersion

$$\frac{1}{G}\frac{d\left(\tilde{\rho}\sigma_r^2\right)}{dr} = -\frac{M\tilde{\rho}}{r^2} \Rightarrow \frac{1}{G}\frac{d\left(\tilde{\rho}\sigma_r^2\right)}{dr} = \frac{1}{dr}\left(\int_r^{\infty}\frac{M\tilde{\rho}}{r'^2}dr'\right) \Rightarrow \sigma_r^2(r) = \frac{G}{\tilde{\rho}}\int_r^{\infty}\frac{M\tilde{\rho}}{r'^2}dr' \tag{A.1.11}$$

Another way to calculate the radial velocity dispersion σ_r^2 is to related it to some kind of temperature measure for dark. Imagine a system with collisional particles (like the gas' particles in the ICM) each with mass m, then the absolute temperature is simply a measure of the kinetic energy:

$$\frac{1}{2}\left\langle v^2\right\rangle = \frac{3}{2}k_BT \Leftrightarrow T = \frac{m}{3k_B}\left\langle v^2\right\rangle \tag{A.1.12}$$

In analogy, we define dark matter's "temperature"[1], and what is the mean-square velocity for collisional particles, we consider the velocity dispersion: $\sigma^2_{DM} = \sigma^2_r + 2\sigma^2_t$ and define the velocity anisotropy ($\beta_{DM} \equiv 1 - \frac{\sigma^2_t}{\sigma^2_r}$), and we can now write,

$$\sigma^2_r = \left[\frac{\mu m_p}{k_B}\left(1 - \frac{2}{3}\beta_{DM}\right)\right]^{-1} T_{DM} \tag{A.1.13}$$

A.2 Relating Gas and DM in clusters

As the gravitational mass for the cluster can be obtained both with Jeans equation (2.1.14) and the hydrostatic equilibrium equation (2.2.9), we can take advantage of this equality and relate the properties of the gas with dark matter in order to create "fake" data that describes the physics of the gas in the ICM.

Deriving gas properties

We start with the NFW profile ($(\alpha, \beta) = (1, 3)$) for dark matter and a Hernquist profile ($(\alpha, \beta) = (1, 4)$) for the gas, see eq. (1.1.1)). We take the total mass as the sum of dark matter and gas mass, which derive from the density assuming spherical symmetry (see section (A.1)).

To calculate the gas temperature we need to assume a profile for the velocity anisotropy of dark matter, for simplicity and also to check if the functions are built correctly we set $\beta = 0$, meaning that dark matter behaves in the same way as a collisional system like the gas in the cluster. We should then expect that the gas and dark matter density profiles should have the same shape: $\gamma_g = \gamma_{dm}$. In this way, the temperature and dispersion velocity squared will be equal up to a proportional factor of $\frac{\mu m_p}{k_B}$.

When we changed the β_{DM} profile to follow $\gamma_{dm} = \frac{d\log\rho_{dm}}{d\log r}$: $\beta(r) = -\frac{1}{6}(1 + \gamma_{dm}(r))$, the derived gas density profile changed with (α, β) given by $\gamma_g = \frac{1}{1-\frac{2}{3}\beta}(\gamma_{DM} + 2\beta_{DM} + \frac{2}{3}\beta_{DM}\frac{d\log\sigma^2_r}{d\log r} + \frac{2}{3}\frac{d\beta_{DM}}{dr})$ [18] and the temperature and velocity dispersion also changes. The latter is shown in fig. A.2.1.

We end up with a new total mass by summing the gas and dark matter masses. We continue with this method until the new gas density profile does not change when comparing with the previous one. To illustrate just this you can follow the flow diagram (A.2.2).

The end result is the one expected, where the final gas density profile follows exactly a NFW, since we considered $\beta_{DM} = 0$ and also a NFW density profile for dark matter.

[1] Quotation marks to remind that the temperature for dark matter is not defined as if it was in thermodynamic equilibrium, since dark matter is collisionless

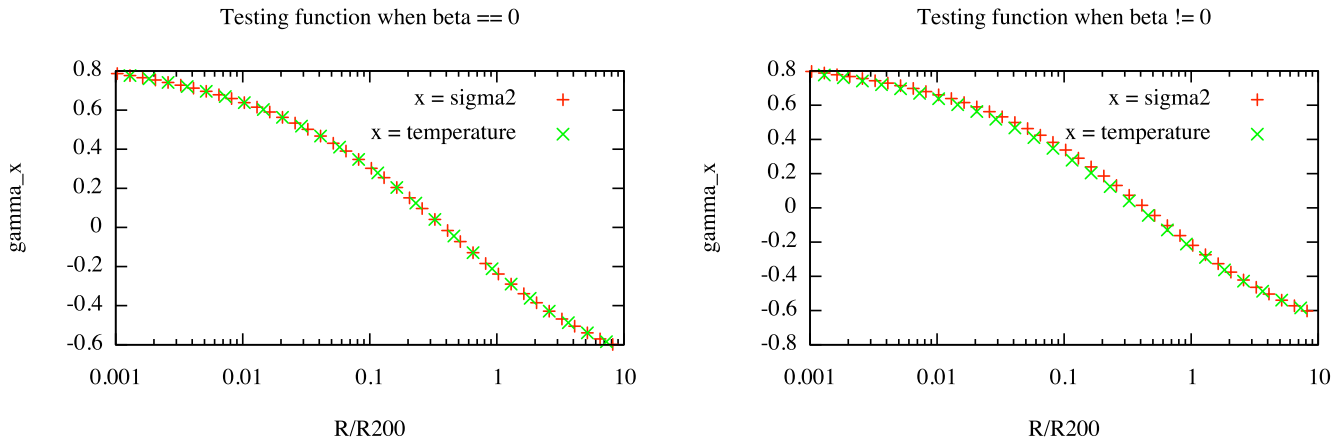

Figure A.2.1: Relation between the gas temperature and the velocity dispersion for dark matter. On the left, the two physical quantities are proportional to each other by a factor of $\frac{\mu m_p}{k_B}$. On the right we have the difference between both, introduced by a different choice of β_{DM}.

Deriving DM properties

Symmetric

Several tests were made to see if everything was doing exactly what we were asking for. The last one was to derive a dark matter profile from the gas which was just derived. We should then expect that we obtain the initial dark matter properties as the one used for the gas if we assume spherical hydrostatic equilibrium. This turned out to be true, as we will now prove.

We assume that all the gravitational contribution comes from the gas and dark matter particles in the cluster: $M_{Total}(r) = M_{DM}(r) + M_g(r)$. The total mass in this case, is estimated from the hydrostatic equilibrium eq.(4.1.1).

Here we write the Jeans' equation, previously derived in Chapter 2.1:

$$M_{Total}(r) = M_{Jeans}(r) = -\frac{r\sigma_r^2(r)}{G}\left(\frac{d\log\rho_{dm}}{d\log r} + \frac{d\log\sigma_r^2}{d\log r} + 2\beta(r)\right) \qquad \text{(A.2.1)}$$

We want to relate the cluster's hydrostatic mass and the Jeans' mass, since they should both give us the cluster's total mass.

If we want to study the Jeans' equation, we see that we need to know about the profiles of the dark matter density, its velocity dispersion and velocity anisotropy. The first can be estimated from the dark matter mass ($M_{DM} = M_{Total} - M_g$) assuming spherical symmetry. We make the assumption that $T_{DM} = T_g$ which then relates to σ^2 by a factor of $k_B/(\mu m_p)$ and take β_{DM} to be zero, note that will later remove the assumption in β_{DM}.

Finally, if our assumption on how the dark matter relates with the gas are correct and if we are lucky to have chosen the correct β_{DM} then, we should expect

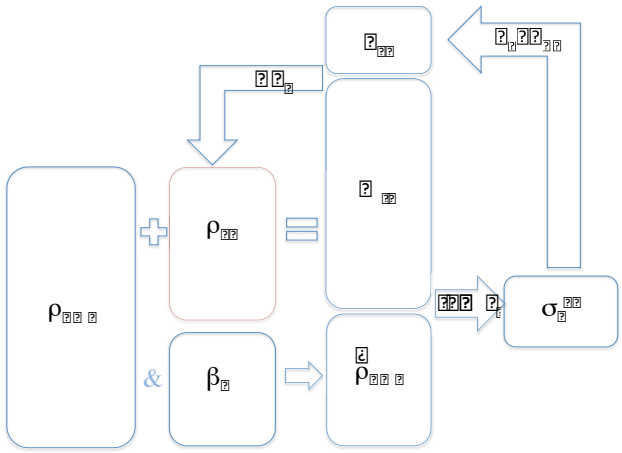

Figure A.2.2: We start by assuming a NFW model for the dark matter density and a Hernquist pro le for the gas. With this we know that $M_{Total} = M_g + M_{DM}$ and we can estimate the temperature from the hydrostatic equilibrium equation. By assuming a pro le for the velocity anisotropy we can calculate the dispersion velocity for dark matter and with that derive the Jeans mass which we take it as the new true mass. With this new mass we can calculate the new gas density from the rst relation and derive a new temperature pro le. We have encountered a loop which will end when the new gas density pro le remains the same as before, meaning that the new gas pro le follows the physics of the cluster.

that $M_{HE} = M_{Jeans} = M_{Total}$. To show numerically the likelihood between these two function, we use the χ^2 as test, ([36]) by calculating the reduced χ^2:

$$\chi^2 = \frac{1}{N} \sum_{i}^{N} \frac{(M_{HE}(r_i) \quad M_{Jeans}(r_i))^2}{\phi^2_{M_{HE}}(r_i) + \phi^2_{M_{Jeans}}(r_i)} \tag{A.2.2}$$

Since we are dealing with numerical data we assumed the associated error to be $\phi_{M_j}(r) = 0\ 1 M_j(r)$.

Note, that we have derived the numerical data for the gas, assuming that we knew about the behaviour of dark matter, that we have taken $_{DM} = 0$. It should then come by no surprise that χ^2 10^{-5}, meaning that the Jeans mass follows exactly the hydrostatic mass[2], q.e.d.

[2]Constraint to the precision in our numerical calculations.

A.3 Numerical calculus

Integral Calculus

The integral of a function $f(x)$ will be calculated numerically by means of the trapeze rule. We define the infinitesimal area at point x_i:

$$\int_{x_{i-1}}^{x_i} f(x_i)dx = Area[f(x_i)] = \frac{1}{2}(x_i - x_{i-1})(f(x_i) + f(x_{i-1})) \tag{A.3.1}$$

this is true for $i = 1, .., N-1$ and $\text{Area}[f(x_i)] = x_i f(x_i)$ when $i = 0$. Finally, the integral of a function is taken, as the sum of all the infinitesimal areas:

$$\int_0^N f(x) = \sum_{i=0}^{N} Area[f(x_i)] \tag{A.3.2}$$

Derivative Calculus

The derivative of a funcion $f(x)$ at a given point x_i will be calculated numerically by taking the average of the segment's slope at x_i and its two first neighbouring points:

$$f'(x_i) = \frac{1}{2}\left(\frac{f(x_i) - f(x_{i-1})}{x_i - x_{i-1}} + \frac{f(x_{i+1}) - f(x_i)}{x_{i+1}) - x_i}\right) \tag{A.3.3}$$

when $i = 0$ or $i = N-1$ we take the derivative equal to the slope between the point at x_i and its first neighbour.

A.4 GNU Scientific Library

This library is important for three reasons:

- "gsl/gsl_const_mksa.h" - access to all physical constants in SI units.
- "gsl/gsl_rng.h" - collection of random number generators. The interface can be found in "libraries/rng.h".
- "gsl/gsl_fit.h" and "gsl/gsl_multifit_nlin.h" - non-linear square fitting. The interface can be found in "libraries/test_fit.h". For each fitting function we also need to calculate the Jacobian. For the minimisation, gsl makes use of the Levenberg-Marquardt algorithm.

A.5 My Library

[3]

[3]This library can be downloaded HERE or in `https://jorge.estamine.net/My_Library_catz.zip`.

Since we are programming in C, we use object-oriented programming. We define two classes in "library/class.h": "array" and "cluster". Each object "array" has an array of bins (N) as a member, each of type "double". Class "cluster" is a collection of "arrays", in it we decide which are our initial conditions, how many entries we wish for the array to have, assign values for maximum and minimum radius as well as the virial radius, and choice of a gas or dark matter profile if desired. We are also given the freedom to create all the parameters that we can help us in defining our cluster, these parameters belonging to class array. Furthermore, we define all sets of functions and routines for the cluster that can be used.

To prevent any memory leaks, it is important to remember deleting the pointers that are no longer needed to run the program. This will also make the program run much faster, avoiding any other conflicts.

array_mathematics.h This library contains the most common operations for and between arrays: copy array to array, set all entries to a certain value, summing arrays, multiplying, sine, calculate the integral or derivative of an array with respect to another array, write an array to a file with x- and y-axis, the list can go on.

array_functions_for_cluster.h Here we will take the operations built in the previous library and construct a set of functions that will return an array according to the mathematics needed for a cluster of galaxies. Some of these functions will be explained in detail.

cluster_set_parameters.h Reads the number of entries of an array, defines parameters as it sets initial values such as minimum and maximum radius.

cluster_make_it_happen.h As the name says, it is where everything for the cluster can happen. We initialise all parameters to value "0" and we can also delete them to free memory. Here is where our cluster begins to take shape. Whenever we want to refer to a certain annulus i, we can do so by using a radial bin notation: r_i, $i = 0, 1, ..., N-1$. The first and last annuli are defined to have a radius equal to r_{min} and r_{max} respectively. As for the other $N-2$ annuli we assign radius such as it follows a logarithmic scale, allowing us a wide range of scales. We define $\Delta r = \frac{1}{N}(\log r_{max} - \log r_{min})$. Therefore, $\log r_i = \log r_{min} + i \times \Delta r \Leftrightarrow r_i = 10^{\log r_i}$. We define all density models for gas and dark matter, calculus of quantities such as γ_j if ρ_j has been calculated and if not one can ask for a density profile. Velocity dispersion and temperature calculus are also available.

cluster_relate_gas_nTh_dm.h In this library, we create functions with the tools developed. With it, we want to be able to determine the gas properties from dark matter and the contribution of non-thermal pressure in the total mass for a given model.

array_fitting_functions.h (& double_fitting_functions.h) Here we have the interface between gsl and the user. With a given set of data points (it can be an array or a pointer to a double) and their standard deviation, we can try to fit this data to a function. We have to write the function and its Jacobian with respect to the fitting parameters.

As an example, we can fit the density to a double power-law given the mass:

$$M(r_i) = 4\pi\rho_0 r_s^\beta \times \int_0^{r_i} r^{2-\alpha}(r+r_s)^{\alpha-\beta}dr \tag{A.5.1}$$

array_error_propagation.h (& double_error_propagation.h) Calculates the error of a given array (vector) (X) given the building parameters (A, B, ...) and respective error. When the parameters are uncorrelated this is easily calculated:

$$\Delta X = \sqrt{|\frac{\partial X}{\partial A}|^2\Delta_A^2 + |\frac{\partial X}{\partial B}|^2\Delta_B^2 + \dots} \tag{A.5.2}$$

read_data_save_to_SI.h Reads the data of choice and writes it to a file in SI units.

optimisation.h We built this routine with searching methods. In particular, we built a sub-routine to find the free-parameters (x_0, x_1) for the bias function, b (see eq. (3.1.4)), which minimise the difference between the total mass of the cluster given the option of the cluster not being in hydrostatic equilibrium, and the total mass of the cluster from the Jeans' equation. The difference between these two masses is given by a measure of χ^2 (defined in eq. (4.1.3)).

We use the successful method of simulated annealing, which is implemented by the *Metropolis algorithm*. The essence of this algorithm is that sometimes, we accept the choice of taking an uphill step, which in our case is a worse χ^2: $\chi^2_{k+1} > \chi^2_k$, allowing us to escape from local minimum and giving us access to a larger region of phase-space. Note that k is defined as the position of the configuration in the Markov chain.

The configuration of a thermodynamical system is defined by a set r_i is weighted by its Boltzmann (probability) factor, $\exp(-E(r_i)/k_BT)$, where $E(r_i)$ is the energy of the set r_i, k_B is the Boltzmann constant and T is the temperature of the thermal bath. To offer the option of taking the uphill or downhill step, the algorithm assigns a probability $w = \exp[-(E_2 - E_1)/k_BT]$. In our case, we want to minimise χ^2, and we change w to become equal to $\Delta\chi^2 = \chi^2_{k+1} - \chi^2_k$.

The Algorithm was implemented as follows:

- Assign how many times you want to generate a new configuration - N_{iter}; the first guess for bias b with free parameters x_0 and x_1 and fixed parameters b_{max} and b_{min}; the step-size δ_r.

- Generate a random configuration for the free parameters in bias: $x_i = x_{i-1} \times 10^{rdm(-\delta_r,\delta_r)}$, $i = 0, 1$. The factor $rdm(-\delta_r, \delta_r)$ is a random number generated uniformly $[-\delta_r, \delta_r]$, given by _rng.h. In this way, the random free parameter will be generated from a logarithmic distribution;

- From this new bias ($b(r)$) calculate the total mass of the cluster, $M_{HE} + \Delta M$, paying attention so that the total mass is bigger than the gas mass at all radii, if not the configuration is rejected as it is not physically possible;

- From the total mass, the gas mass, density and temperature, calculate the dark matter properties and derive the Jeans' mass.

- Calculate the new χ^2 from eq.(4.1.3);

- If the new $\chi^2_k \leqslant \chi^2_{k-1}$ we accept the new configuration;

- If not, then we assign a probability r[4] and compare with $w = exp{-}1/2(\Delta\chi^2)$:

  - If $r > w$ - accept the new configuration
  - Else - reject the new configuration by keeping the old one. We decrease the step-size so that we do not end with more than 50% of rejections.

- Repeat from the second step N_{iter} times.

We also develop the Genetic Algorithm, even though the Metropolis is already very powerful avoiding getting trapped in local minimum by assigning a probability w of escaping from it. The advantage of using the Genetic Algorithm is that it mixes our testing function, introducing mutations. At each run we start with a family of functions and for each member we apply a simple Monte Carlo Algorithm. The best two members (for which chi^2 is less than the other members) will be mixed again and the process will start over. We stop when we see fit. The advantage of this algorithm is that it goes through most of phase-space quite fast because it mixes the sample and can easily get out of a local minimum. Nevertheless, we did not have time to test if this was the best option since the Metropolis worked quite well.

[4]Generate a random number uniformly distributed between 0 and 1 with _rng.h.

Appendix B

Observations

B.1 X-ray spectrum

The observation of the continuum part of the spectrum from X-ray radiation (see Fig.1.2.1) is due to "Bremsstrahlung" effect, when a charged particle is deflected from its inertial movement and emits electromagnetic radiation. The movement of such particles changes due to the Coulomb interaction with an electric field from an atomic nucleus. As the charge is deflected, it will accelerate resulting on the emission of a photon, and the photon's energy will be proportional to the difference in the charged particle's kinetic energy: $h\nu = K_i - K_f$.

The X-ray spectrum shows spectral lines. These emission lines are related to the metallicity of the cluster as it corresponds to the electronic transitions in the atom. Moseley established a relation between a spectral line's characteristic wavelength $\bar{\nu_l}$ with the atomic number Z of the element:

$$\bar{\nu_l} = C_l(Z - s) \tag{B.1.1}$$

where C_l is a constant and the value of s depends on whether it is a K or L line.

Since we know the spectral lines' wavelength in the lab rest-frame, it is possible to estimate the cluster's redshift by measuring the 7keV line for iron (Fe). We should observe a change in the wavelength from the Doppler effect.

B.2 Cosmic Rays spectrum

Synchrotron spectrum

The main process at the origin of the radio emission in the universe is due to the synchrotron process. As relativistic electrons spiral in the presence of a magnetic field frozen in the ICM they emit radiation. An electron with energy $E = \gamma m_e c^2$, experiences a force $\mathbf{F} = \mathbf{v} \times \mathbf{B}$ and emits radiation. Given the large number of relativistic electrons in radio sources, the radiation will be observed as a continuum signal, with a spectrum peaked near the frequency ν, [34]:

$$\nu_{syn} = \frac{3e}{4\pi m_e^3 c^5}(B\sin\theta)E^2 \tag{B.2.1}$$

where θ is the pitch angle between the electron velocity and the magnetic field direction. The power emitted by a relativistic electron,

$$\frac{dE}{dt} = -\frac{2e^4}{3m_e^4 c^7}(B\sin\theta)E^2 \tag{B.2.2}$$

Which substituting in eq.(B.2.1) gives

$$\nu_{syn}[MHz] \sim 16\times 10^6 (B_{[G]}\sin\theta)E^2_{[GeV]} \Leftrightarrow \tag{B.2.3}$$

$$\nu_{syn}[MHz] \sim 4.2(B_{[G]}\sin\theta)\gamma^2 \tag{B.2.4}$$

This tell us that relativistic electrons ($\gamma \sim -10^3 - 10^4$) moving in a region with magnetic field of the order of μG radiate in the radio domain (30kHz-300GHz).

B.3 Measuring the intensity of magnetic fields

There are different methods used to estimate the intensity of the magnetic field in the ICM. These are from observation of the Faraday rotation effect, the comparison of the synchrotron radiation fluxes with inverse Compton X-ray emission and with equipartition measurements.

With these three different methods, we get different magnetic field intensity estimations on a range from 0.1μ G to 10μ G. This is because the magnetic field in the ICM has quite complex structures at different scales, and the different methods rely on different assumptions. We will put emphasis on the Faraday effect.

Faraday Effect

To understand the physics behind the Faraday effect we took as reference the discussion in Hecht [22].

Light travelling inside a bi-refrigent material can be influenced by an external magnetic field as the material will interact with the right- and left-circular polarised component of the light beam with different refractive indices. A consequence of this will be a change in the relative phase-shift between the two circular components, thus there will be a rotation in the position angle of polarisation. This phenomena was discovered in 1845 by Michael Faraday. When testing this effect in materials, the rotation angle β of the vibration plane is given by the empirical expression: $\beta = VBd$ with V being Verdet's constant, B density of the magnetic flux and d the distance that light travelled inside the medium.

With the discovery of the Faraday rotation effect associated with the polarised radiation from radio sources in galaxies and galaxy clusters (since magnetised plasma is optically bi-refringent), it is possible to have some information on the distribution

of free electrons and magnetic fields both in the source itself and along the line of sight between the source and the observer. For this reason, it seems clear that the more RM we have from different radio sources placed within and behind the cluster at different radii with respect to the cluster centre, the better we know about how the magnetic field behaves inside the cluster.

Rotation Measurement

As we will see, by analysing the polarised emission of radio sources within the cluster it is possible to estimate the average magnetic field. The polarised signal is described by the polarisation vector (p), whose intensity (P) and angle (χ) are given by (Murgia et al. 2004)

$$P = \sqrt{Q^2 + U^2} \tag{B.3.1}$$

$$\chi = \frac{1}{2} \tan^{-1} \frac{U}{Q} \tag{B.3.2}$$

where Q and U are the Stokes parameters (see section (B.3) for details about Stokes parameters) and the polarisation degree can be evaluated as P/I where I is the total intensity. The presence of a magnetised plasma between the observer and a radio source changes the properties of the polarised signal due to the Faraday effect. The polarisation vector rotates while crossing a magnetised and ionised plasma according to the λ^2 law:

$$\Delta\chi = RM \frac{\lambda^2}{(1+z)^2} \tag{B.3.3}$$

where $\Delta\chi = \chi_{obs}(\lambda) - \chi_{int}$ is the difference between the polarisation angle observed at a wavelength λ, z is the redshift of the Faraday screen and RM is the rotation measure that depends on the magnetic field strength of the medium $\mathbf{B}[\mu G]$, as well as the number density of free (thermal) electrons $n_e[cm^{-3}]$, along the line-of-sight:

$$RM \sim \int n_e \mathbf{B} \cdot d\mathbf{l} \quad [radm^{-2}] \tag{B.3.4}$$

the factor of proportionality being $e^3/2\pi m^2 c^4$ and the integral is taken over the the distance from the source to the observer (in kpc) [6]. From observations from radio sources, we are given a RM map and from X-ray analysis we know $n_e(r)$, it should then be possible to know something about the magnetic field along the line-of-sight. However, due to the random character of the magnetic field in the cluster, eq.(B.3.4) is not analytically solvable [28], and one usually takes an average of the field to determine the power spectra. This is by far an oversimplification of the

problem and other more complex methods are proposed such as Fourier transforming the RM[1].

Mathematical description of polarisation

The state of polarisation is given by the Stokes parameters $(S_0, S_1, S_2, S_3) = (I, Q, U, V)$ that can be defined as:

$$\begin{aligned} S_0 &= 2I_0 \\ S_1 &= 2(I_1 - I_0) \\ S_2 &= 2(I_2 - I_0) \\ S_3 &= 2(I_3 - I_0) \end{aligned} \tag{B.3.5}$$

S_0 is irradiance and $S_1,\ S_2,\ S_3$ specify the state of polarisation. To determine experimentally the state of polarisation of an arbitrary beam of electromagnetic radiation, four sets of experiments need to be carried out providing us with information about the intensity of the beam: i) & ii) the degree of plane polarisation with respect to two arbitrary orthogonal axes, iii) the degree of plane polarisation with respect to a set of axes oriented at 45° to the right of the previous one and iv) the degree of circular polarisation. In optics, we can measure the polarisation by measuring the radiation transmitted when applying one of the four different filters: isotropic, linear polariser on the 1^{st} and 3^{rd} quadrant and circular polariser to the incoming light, giving us I_i with $i = 0,\ 1,\ 2,\ 3$, respectively.

We define monochromatic radiation:

$$\begin{aligned} E_x(t) &= E_{0x}(t)\cos\left[(\bar{k}z - \bar{\omega}t)\right] \\ E_y(t) &= E_{0y}(t)\cos\left[(\bar{k}z - \bar{\omega}t)\right] \end{aligned} \tag{B.3.6}$$

where $\bar{k}$ and $\bar{\omega}$ correspond to the average of the values associated with the wave spectrum. When we have a detector, the measured value will be an average over time. In this way, Stokes parameters can written as

$$\begin{aligned} I = S_0 &= \langle E_{0x}^2 \rangle + \left\langle E_{0y}^2 \right\rangle = \sqrt{Q^2 + U^2 + V^2} \\ Q = S_1 &= \langle E_{0x}^2 \rangle - \left\langle E_{0y}^2 \right\rangle = I\cos 2\beta \cos 2\theta \\ U = S_2 &= \langle 2E_{0x}E_{0y}\cos\epsilon \rangle = I\cos 2\beta \sin 2\theta \\ V = S_3 &= \langle 2E_{0x}E_{0y}\sin\epsilon \rangle = I\sin 2\beta \end{aligned} \tag{B.3.7}$$

If we normalise it, we can represent natural light as $(I, Q, U, V) = (1, 0, 0, 0)$ and we will do so from now on. β is the angle whose tangent is the ratio of the two axes of the polarised ellipse and in the case of circular polarisation $\beta = n\frac{\pi}{4},\ n = 1, 2, ...$ which makes $V = \sqrt{2}I$ and when we have linear polarisation $\beta = n\pi,\ n = 0, 1, ...$ leading to $V = 0$.

[1]For such studies one can read for example, Enßlin & Vogt [16].

Inverse Comption scattering

The Inverse Compton scattering, is of course, the inverse of the Compton scattering. In Compton scattering, we study the physics of high energy photons' transfer of energy and momentum to non-relativistic electrons. This makes the photon's wavelength increase. In Inverse Compton scattering, we study the case of relativistic electrons colliding with low-energy photons. After the collision, energy is transferred from the electron to the photon. Relating this with our problem, we have that the photons are emitted in the radio-band from synchrotron emission, when the magnetic field accelerates the CR electrons. These electrons will then collide with the same emitted photons. From this scattering, the photons will gain energy up to the X-ray-band.

We can make an estimation on the magnetic field strength, relating the energy emitted by synchrotron radiation and the inverse Compton effect by the same electron distribution:

$$\frac{\left(\frac{dE}{dt}\right)|_{sync}}{\left(\frac{dE}{dt}\right)|_{ic}} = \frac{B^2}{2\mu_0}\frac{1}{U_\epsilon} \tag{B.3.8}$$

where here B is the magnetic flux density in the source region and U_ϵ is the energy density of radiation.

B.4 Measuring the velocity for the gas

Sunyaev et al. [39], consider observing the gas motion of galaxy clusters via:

Doppler Broadening and Shifting of Emission Lines This technique needs high-resolution the observations of the X-ray spectrum of galaxy clusters[2]. It is expected that with such resolution it becomes possible to measure the Doppler shift of the iron emission lines [38]:

$$\Delta\lambda \approx \frac{0.124}{m}\Delta\theta\mathring{A} \tag{B.4.1}$$

where m is the spectral order and $\Delta\theta$ is the half energy width of the source in arcmin. The observed broadening is the sum of the spatial broadening ($\Delta\lambda$), the thermal broadening of the ICM and any turbulent motions within that region. We see a problem with this choice, it seems to be sensitive to the Doppler effect, with this we mean that we can only measure the velocity of the gas that is transverse along the line-of-sight. The resolution of today's telescopes does not allow to measure this velocity. Sanders et al. [38], try to do so. However, we can not trust their results as they give their results lacking on precision and accuracy (their error-bars are sometimes even larger than the given value).

[2]ALMA (Atacama Large millimeter array) can potentially give the high-resolution needed for this task.

SZ effect The SZ effect is the same as the inverse Compton scatter (app. B.3), with the particularity that in this case, we have CMB photons colliding with the hot gas in the ICM. After collision, these low energy photons are boosted to higher frequencies, distorting the Planck blackbody spectrum. This distortion in the spectrum is related to the measurement of y, the line-of-sight integral of the gas pressure through the ICM:

$$\frac{\Delta T}{T} = -2y$$

and

$$y = \int_{-\infty}^{\infty} \frac{k_B T_e}{m_e c^2} \sigma_T n_e dl$$

with T_e, m_e and n_e being the electron temperature, mass and number density, σ_T is the Thompson scattering cross section. From this effect we will have a total temperature decrement, which is the sum of the thermal and the kinematic (SZ) effect of the gas in the ICM. The first corresponds for the the inverse Compton scattering of the CMB photons with the plasma, and can be proposed to be measured with the spectral lines. The latter, corresponds to the turbulent motion of the cluster. The scattering of CMB will suffer Doppler shift from the radial velocity of the gas along the line-of-sight, and the shift in temperature is related with the fluid velocity along the line-of-sight. Measuring the kinematic SZ, is below current limits of detectability [39].

Appendix C

Mathematical background

We take as reference, Arfken [2].

C.1 Spherical Coordinates

In spherical coordinates, we make use of the convention (r, θ, ϕ): $r \in [0, \infty[$, $\theta \in [0, 2\pi]$ and $\phi \in [0, \pi]$. In this way we can write the position vector as

$$\mathbf{r} = r(\cos\theta \sin\phi, \sin\theta \sin\phi, \cos\phi) \tag{C.1.1}$$

A unit vector can be defined in the general form by $\hat{e}_i = \dfrac{\dfrac{\partial \mathbf{r}}{\partial x_i}}{\left|\dfrac{\partial \mathbf{r}}{\partial x_i}\right|}$. In this way we can write our unit vectors in spherical coordinates:

$$\hat{e}_r = (\cos\theta \sin\phi, \sin\theta \sin\phi, \cos\phi) \tag{C.1.2}$$
$$\hat{e}_\theta = (-\sin\theta, \cos\theta, 0) \tag{C.1.3}$$
$$\hat{e}_\phi = (\cos\theta \cos\phi, \sin\theta \cos\phi, -\sin\phi) \tag{C.1.4}$$

It can easily be shown that the rate of change of the unit vectors can be written in the following way where $\dot{x}$ is just the time derivative of x:

$$\dot{\hat{e}}_r = \dot{\theta} \sin\phi \hat{e}_\theta + \dot{\phi} \hat{e}_\phi \tag{C.1.5}$$
$$\dot{\hat{e}}_\theta = -\dot{\theta} \sin\phi \hat{e}_r - \dot{\theta} \cos\phi \hat{e}_\phi \tag{C.1.6}$$
$$\dot{\hat{e}}_\phi = -\dot{\phi} \hat{e}_r + \dot{\theta} \cos\phi \hat{e}_\theta \tag{C.1.7}$$

From (C.1.1) we can derive the velocity $\mathbf{v} = (v_r, v_\theta, v_\phi) = \dfrac{d\mathbf{r}}{dt} = \hat{e}_r \dot{r} + \dot{\hat{e}}_r r$:

$$\mathbf{v} = \dot{r} \hat{e}_r + r\dot{\theta} \sin\phi \hat{e}_\theta + r\dot{\phi} \hat{e}_\phi = \tag{C.1.8}$$

In the same way we can derive the acceleration $\mathbf{a} = (a_r, a_\theta, a_\phi) = \frac{d\mathbf{v}}{dt} = \dot{v}_r\hat{e}_r + v_r\dot{\hat{e}}_r + \dot{v}_\theta\hat{e}_\theta + v_\theta\dot{\hat{e}}_\theta + \dot{v}_\phi\hat{e}_\phi + v_\phi\dot{\hat{e}}_\phi$:

$$\mathbf{a} = \left(\dot{v}_r - \frac{(v_\theta^2 + v_\phi^2)}{r}\right)\hat{e}_r + \tag{C.1.9}$$

$$\left(\frac{v_r v_\theta}{r} + \dot{v_\theta} + v_\phi\dot{\theta}\cos\phi\right)\hat{e}_\theta + \tag{C.1.10}$$

$$\left(\frac{v_r v_\phi}{r} + \dot{v}_\phi - v_\theta\dot{\theta}\cos\phi\right)\hat{e}_\phi \tag{C.1.11}$$

The gradient can be written in the general form for any orthogonal coordinate system $\boldsymbol{\nabla} = \frac{\hat{e}_i}{\sqrt{g_{ii}}}\frac{\partial}{\partial x_i}$ and as the metric g_{ij} in spherical coordinates is

$$g_{ij} = \begin{pmatrix} 1 & 0 & 0 \\ 0 & r^2\sin^2\phi & 0 \\ 0 & 0 & r \end{pmatrix} \tag{C.1.12}$$

We can explicitly write the gradient in this coordinate system:

$$\boldsymbol{\nabla} = \hat{e}_r\frac{\partial}{\partial r} + \frac{\hat{e}_\theta}{r\sin\phi}\frac{\partial}{\partial\theta} + \frac{\hat{e}_\phi}{r}\frac{\partial}{\partial\phi} \tag{C.1.13}$$

The divergence of a vector $\mathbf{F} = (F_r, F_\theta, F_\phi)$ is

$$\boldsymbol{\nabla}\cdot\mathbf{F} = \frac{1}{r^2}\frac{\partial}{\partial r}\left(r^2F_r\right) + \frac{1}{r\sin\phi}\frac{\partial F_\theta}{\partial\theta} + \frac{1}{r\sin\phi}\frac{\partial}{\partial\phi}\left(\sin\phi F_\phi\right) \tag{C.1.14}$$

The curl in spherical coordinates, where $F = (F_r, F_\theta, F_\phi)$ is

$$\boldsymbol{\nabla}\times F = \frac{1}{r\sin\phi}\left[\frac{\partial}{\partial\phi}\left(\sin\phi F_\theta\right) - \frac{\partial F_\phi}{\partial\theta}\right]\hat{e}_r + \tag{C.1.15}$$

$$\frac{1}{r}\left[\frac{\partial}{\partial r}\left(rF_\phi\right) - \frac{\partial F_r}{\partial\phi}\right]\hat{e}_\theta + \tag{C.1.16}$$

$$\frac{1}{r}\left[\frac{1}{\sin\phi}\frac{\partial F_r}{\partial\theta} - \frac{\partial}{\partial r}\left(rF_\theta\right)\right]\hat{e}_\phi \tag{C.1.17}$$

C.2 Divergence theorem

$$\int_V (\nabla\cdot\mathbf{F})\,dV = \oint_S \mathbf{F}\cdot d\mathbf{S} \tag{C.2.1}$$

Physically, this theorem states that in the absence of the creation or destruction of matter, the density within a region of space can change only by having it flow into or away from the region through its boundary.

Appendix D

Abbreviations

AGN active galactic nuclei

CBE collisionless Boltzmann equation

CC cool core clusters

CDM cold dark matter

CMB cosmic microwave background

CR cosmic ray

DF distribution function

FR Faraday rotation

FRM Faraday rotation measurement

FRW Friedmann–Robertson–Walker

HE Hydrostatic equilibrium

IC inverse Compton

ICM intra-cluster medium

LHS left-hand side

NCC non-cool core clusters

NFW Navarro-Frenk-White

RHS right-hand side

RM rotation measurement

Bibliography

[1] Shin'ichiro Ando and Daisuke Nagai. Gamma-ray probe of cosmic-ray pressure in galaxy clusters and cosmological implications. 05 2007.

[2] G. Arfken. *Mathematical Methods for Physicists*. Orlando, FL Academic Press, 1985.

[3] A.Vikhlinin, A.V.Kravtsov, R.A.Burenin, H.Ebeling, W.R.Forman, A.Hornstrup, C.Jones, S.S.Murray, D.Nagai, H.Quintana, and A.Voevodkin. Chandra cluster cosmology project iii: Cosmological parameter constraints. 12 2008.

[4] James Binney and Scott Tremaine. *Galactic Dynamics*. Princeton Press, 2nd. edition, 2008.

[5] Elizabeth L. Blanton, Craig L. Sarazin, and Brian R. McNamara. Chandra observation of the cooling flow cluster abell 2052. *Astrophys.J.*, 585:227–243, 2003.

[6] A. Bonafede, L. Feretti, M. Murgia, F. Govoni, G. Giovannini, D. Dallacasa, K. Dolag, and G. B. Taylor. The coma cluster magnetic field from faraday rotation measures. 2010.

[7] Stefano Borgani. Cosmology with clusters of galaxies. 2006.

[8] T. J. M. Boyd and J.J. Sanderson. *The Physics of Plasmas*. Cambridge University Press, 2003.

[9] G. Brunetti. Non-thermal emission from galaxy clusters and future observations with the fermi gamma-ray telescope and lofar. 2008.

[10] Jack O. Burns. The radio properties of cd galaxies in abell clusters. i - an x-ray selected sample. *Astronomical Journal*, 99:14–30, 1990.

[11] A. Cavaliere and R. Fusco-Femiano. X-rays from hot plasma in clusters of galaxies. *Astron. and Astrophys.*, 49(137), 1976.

[12] Scott Dodelson. *Modern Cosmology*. Academic Press, 2003.

[13] K. Dolag, A.M. Bykov, and A. Diaferio. Non-thermal processes in cosmological simulations. 2008.

[14] K. Dolag, S. Schindler, F. Govoni, and L. Feretti. 2001. *Astron. and Astrophys.*, 378(777).

[15] F. Durret, G. B. Lima Neto, and W. Forman. *Astron. and Astrophys.*, 432(80), 2005.

[16] T. A. Ensslin and C. Vogt. The magnetic power spectrum in faraday rotation screens. *Astron. and Astrophys.*, 401(835), 2003.

[17] Andrey V. Kravtsov Erwin T. Lau and Daisuke Nagai. Residual gas motions in the intracluster medium and bias in hydrostatic measurements of mass profiles of clusters. 2009.

[18] Teddy F. Frederiksen, Steen H. Hansen, Ole Host, and Marco Roncadelli. Determining all gas properties in galaxy clusters from the dark matter distribution alone. 06 2009.

[19] Ken Freeman and Geoff McNamara. *In Search of Dark Matter*. Springer Praxis Books, 2006.

[20] Steen H. Hansen and Rocco Piffaretti. Measuring the dark matter velocity anisotropy in galaxy clusters. 2007.

[21] Jiangang Hao and James Annis. Flying across galaxy clusters with google earth: additional imagery from sdss co-added data. 2010.

[22] Eugene Hecht. *Optics*. Addison Wesley, 4th edition, 2002.

[23] Ole Host, Steen H. Hansen, Rocco Piffaretti, Andrea Morandi, Stefano Ettori, Scott T. Kay, and Riccardo Valdarnini. Measurement of the dark matter velocity anisotropy in galaxy clusters. 08 2008.

[24] Naomi Kawano and Yasushi Fukazawa. Chandra observations of the central cool region of galaxy clusters. *Advances in Space Research*, 36:605–610, 2005.

[25] Russell M. Kulsrud and Ellen G. Zweibel. On the origin of cosmic magnetic fields. 07 2007.

[26] T. F. Laganá, R. S. de Souza, and G. R. Keller. On the influence of non-thermal pressure on the mass determination of galaxy clusters. *Astron. and Astrophys.*, 510:A76, 2010.

[27] L. D. Landau and E. M. Lifshitz. *Fluid mechanics - volume 6: course of theoretical physics*. Butterworth-Heinemann, 2nd. edition, 1987.

[28] M. Murgia, F. Govoni, G. Feretti, L.and Giovannini, D. Dallacasa, R. Fanti, G. B. Taylor, and K. Dolag. Magnetic fields and faraday rotation in clusters of galaxies. *Astron. and Astrophys.*, 424:429–446, 2004.

[29] Julio F. Navarro, Carlos S. Frenk, and Simon D.M. White. The structure of cold dark matter halos. *Astrophys.J.*, 462:563–575, 1996.

[30] M.L. Norman and G.L. Bryan. Numerical astrophysics 1998. *Astrophysics and Space Science Library*, 240(19), 1999.

[31] E. Orru, M. Murgia, L. Feretti, F. Govoni, G. Brunetti, G. Giovannini, M. Girardi, and G. Setti. Low-frequency study of two clusters of galaxies: A2744 and a2219. *Astron. and Astrophys.*, 467(943-954), 2007.

[32] Christoph Pfrommer and Torsten A. Ensslin. Constraining the population of cosmic ray protons in cooling flow clusters with gamma-ray and radio observations: Are radio mini-halos of hadronic origin? *Astron. and Astrophys.*, 426:777–777, 2004.

[33] Rocco Piffaretti, Philippe Jetzer, Jelle Kaastra, and Takayuki Tamura. Temperature and entropy profiles of nearby cooling flow clusters observed with xmm-newton. *Astron.Astrophys.*, 433:101–111, 2005.

[34] Roberto Francesco Pizzo. *Tomography of galaxy clusters through low-frequency radio polarimetry*. University of Groningen, 2010.

[35] E. Pointecouteau, M. Arnaud, J. Kaastra, and J. de Plaa. Xmm-newton observation of the relaxed cluster a478. *Astron.Astrophys.*, 423:33–47, 2004.

[36] William H. Press, Saul A. Teukolsky, William T. Vetterling, and Brian P. Flannery. *Numerical Recipes in C*. Cambridge University Press, 2nd. edition, 1992.

[37] Signe Riemer-Sorensen, Danka Paraficz, Desiree Della Monica Ferreira, Kristian Pedersen, Marceau Limousin, and Haakon Dahle. Resolving the discrepancy between lensing and x-ray mass estimates of the complex galaxy cluster abell 1689. 11 2008.

[38] J.S. Sanders, A.C. Fabian, and R.K. Smith. Constraints on turbulent velocity broadening for a sample of clusters, groups and elliptical galaxies using xmm-newton. 08 2010.

[39] R. A. Sunyaev, M. L. Norman, and G. L. Bryan. On the detectability of turbulence and bulk flows in x-ray clusters. *Astronomy Letters*, 29:783–790, 2003.

[40] A. Vikhlinin, A. Kravtsov, W. Forman, C. Jones, M. Markevitch, S. S. Murray, and L. Van Speybroeck. Chandra sample of nearby relaxed galaxy clusters: mass, gas fraction, and mass-temperature relation. *Astrophys.J.*, 640:691–709, 2006.

[41] G. Mark Voit. Tracing cosmic evolution with clusters of galaxies. *Rev.Mod.Phys.*, 77:207–258, 2005.

[42] Hao Xu, Brian W. O'Shea, David C. Collins, Michael L. Norman, Hui Li, and Shengtai Li. The biermann battery in cosmological mhd simulations of population iii star formation the biermann battery in cosmological mhd simulations of population iii star formation the biermann battery in cosmological mhd simulations of population iii star formation. *The Astrophysical Journal*, 688, 2008.

[43] Yu-Ying Zhang, Nobuhiro Okabe, Alexis Finoguenov, Graham P. Smith, Rocco Piffaretti, Riccardo Valdarnini, Arif Babul, August E. Evrard, Pasquale Mazzotta, Alastair J.R. Sanderson, and Daniel P. Marrone. Locuss: A comparison of cluster mass measurements from xmm-newton and subaru - testing deviation from hydrostatic equilibrium and non-thermal pressure support. 2010.